

SIMULATION OF CONJUGATE HEAT TRANSFER PROBLEMS USING
LEAST SQUARES FINITE ELEMENT METHOD

A THESIS SUBMITTED TO
THE GRADUATE SCHOOL OF NATURAL AND APPLIED SCIENCES
OF
MIDDLE EAST TECHNICAL UNIVERSITY

BY

MUSTAFA UĞUR GÖKTOLGA

IN PARTIAL FULFILLMENT OF THE REQUIREMENTS
FOR
THE DEGREE OF MASTER OF SCIENCE
IN
MECHANICAL ENGINEERING

SEPTEMBER 2012

Approval of the thesis :

**SIMULATION OF CONJUGATE HEAT TRANSFER PROBLEMS USING
LEAST SQUARES FINITE ELEMENT METHOD**

submitted by **MUSTAFA UĞUR GÖKTOLGA** in partial fulfillment of the requirements for the degree of **Master of Science in Mechanical Engineering Department, Middle East Technical University** by,

Prof. Dr. Canan Özgen
Dean, Graduate School of **Natural and Applied Sciences**

Prof. Dr. Suha Oral
Head of Department, **Mechanical Engineering**

Asst. Prof. Dr. Cüneyt Sert
Supervisor, **Mechanical Engineering Dept., METU**

Examining Committee Members:

Prof. Dr. Mehmet Haluk Aksel
Mechanical Engineering Dept., METU

Asst. Prof. Dr. Cüneyt Sert
Mechanical Engineering Dept., METU

Assoc. Prof. Dr. Almıla Güvenç Yazıcıoğlu
Mechanical Engineering Dept., METU

Asst. Prof. Dr. Ahmet Yozgatlıgil
Mechanical Engineering Dept., METU

Asst. Prof. Dr. Barbaros Çetin
Mechanical Engineering Dept., Bilkent University

Date: 11.09.2012

I hereby declare that all information in this document has been obtained and presented in accordance with academic rules and ethical conduct. I also declare that, as required by these rules and conduct, I have fully cited and referenced all material and results that are not original to this work.

Name, Last name: Mustafa Uğur Göktolga

Signature :

ABSTRACT

SIMULATION OF CONJUGATE HEAT TRANSFER PROBLEMS USING LEAST SQUARES FINITE ELEMENT METHOD

Göktolga, Mustafa Uğur

M.S., Department of Mechanical Engineering

Supervisor : Asst. Prof. Dr. Cüneyt Sert

September 2012, 79 pages

In this thesis study, a least-squares finite element method (LSFEM) based conjugate heat transfer solver was developed. In the mentioned solver, fluid flow and heat transfer computations were performed separately. This means that the calculated velocity values in the flow calculation part were exported to the heat transfer part to be used in the convective part of the energy equation. Incompressible Navier-Stokes equations were used in the flow simulations. In conjugate heat transfer computations, it is required to calculate the heat transfer in both flow field and solid region. In this study, conjugate behavior was accomplished in a fully coupled manner, i.e., energy equation for fluid and solid regions was solved simultaneously and no boundary conditions were defined on the fluid-solid interface. To assure that the developed solver works properly, lid driven cavity flow, backward facing step flow and thermally driven cavity flow problems were simulated in three dimensions and the findings compared well with the available data from the literature. Couette flow and thermally driven cavity flow with conjugate heat transfer in two dimensions were modeled to further validate the solver. Finally, a microchannel conjugate heat transfer problem was simulated. In the flow solution part of the microchannel problem, conservation of mass was not achieved. This problem was expected since the LSFEM has problems related to mass conservation especially in high aspect ratio channels. In order to overcome the mentioned problem, weight of continuity equation was increased by multiplying it with a constant. Weighting worked for the microchannel problem and the mass conservation issue was resolved. Obtained

results for microchannel heat transfer problem were in good agreement in general with the previous experimental and numerical works.

In the first computations with the solver; quadrilateral and triangular elements for two dimensional problems, hexagonal and tetrahedron elements for three dimensional problems were tried. However, since only the quadrilateral and hexagonal elements gave satisfactory results, they were used in all the above mentioned simulations.

Keywords: Least-Squares Finite Element Method, Conjugate Heat Transfer, Microchannel Heat Transfer, Incompressible Viscous Flows, Navier-Stokes Equations

ÖZ

EN KÜÇÜK KARELER SONLU ELEMAN YÖNTEMİ KULLANILARAK EŞLENİK ISI TRANSFERİ PROBLEMLERİNİN BENZETİMİ

Göktolga, Mustafa Uğur

Yüksek Lisans, Makina Mühendisliği Bölümü

Tez Yöneticisi : Yrd. Doç. Dr. Cüneyt Sert

Eylül 2012, 79 sayfa

Bu tez çalışmasında, en küçük kareler sonlu eleman yöntemi (EKKSEY) tabanlı bir eşlenik ısı transferi çözücüsü geliştirilmiştir. Bahsedilen çözücüde, akış ve ısı transferi hesaplamaları ayrı ayrı yapılmıştır. Bu, akışkan çözücü kısmında hesaplanan hız değerlerinin, ısı transferi çözücüsündeki enerji denkleminin taşınım kısmında kullanılması manasına gelmektedir. Akışkan çözümlerinde sıkıştırılamayan Navier-Stokes denklemleri kullanılmaktadır. Eşlenik ısı transferi çözümlerinde, hem katı hem de sıvı kısımlar için ısı transferinin hesaplanması gerekmektedir. Bu çalışmada, eşlenik davranış sıkı bağlı bir şekilde modellenmiştir. Yani, enerji denklemi sıvı ve katı kısımlar için aynı anda çözülmüş ve sıvı-katı arayüzü için ayrıca sınır koşulları tanımlanmamıştır. Geliştirilen çözücünün düzgün bir şekilde çalıştığından emin olabilmek için; kapakla hareket ettirilen kavite akışı problemi, geriye dönük basamak akışı problemi ve ısıyla hareket ettirilen kavite akışı probleminin üç boyutta benzetimleri yapılmış ve bulgular literatürde bulunan verilerle örtüşmüştür. Çözücüyü daha da doğrulamak için, eşlenik ısı transferi içeren iki boyutlu Couette akışı ve ısı ile hareket ettirilen kavite akışı modellenmiştir. Son olarak, bir mikrokanal eşlenik ısı transferi probleminin benzetimi yapılmıştır. Mikrokanal probleminin akış çözümünde kütle korunumu sağlanamamıştır. EKKSEY'in özellikle yüksek açıklık oranına sahip kanallarda kütle korunumuyla alakalı problemleri olduğu bilindiğinden, bu tarz bir problemle karşılaşmak zaten beklenmektedir. Belirtilen problemi aşmak için, süreklilik denkleminin ağırlığı, bir katsayıyla çarpılarak artırılmıştır. Ağırlık artırma mikrokanal problemi için işe

yaramış ve kütle korunumu sıkıntısı giderilmiştir. Mikrokanal problemi için elde edilen sonuçlar, daha önce yapılan deneysel ve sayısal çalışmalarla örtüşmektedir.

Çözücüyle yapılan ilk hesaplamalarda; iki boyutta dört yüzlü ve üçgen elemanlar, üç boyutta ise altı yüzlü ve dört yüzlü (üçgen piramit) elemanlar kullanılmıştır. Fakat, iki boyutta sadece dört yüzlü, üç boyutta ise sadece altı yüzlü elemanlar tatmin edici sonuçlar verdiğiinden, yukarıda bahsedilen tüm benzetimlerde bu elemanlar kullanılmıştır.

Anahtar Kelimeler: En Küçük Kareler Sonlu Eleman Yöntemi, Eşlenik Isı Transferi, Mikrokanal Isı Transferi, Sıkıştırılmayan Ağdalı Akışlar, Navier-Stokes Denklemleri

To my family

ACKNOWLEDGMENTS

I would like to thank my thesis supervisor, Dr. Cüneyt Sert, for his encouragement, support and guidance. Without him, this thesis could not be as improved as it is now.

I would like to express my gratitude to my family for their unconditional love. Awareness of being loved no matter what you do must be the most comforting feeling in the world.

I want to thank my company, Roketsan, for supporting me in obtaining a Master's degree. I also want to thank my colleagues at Roketsan, especially Yiğit Akargün, for their contributions and encouragements.

I am thankful to my friends Suat Ertuğrul, Bilgin Navruz, Emre Topbaş and Merve Okatan for their supply in various ways.

Lastly, I want to express my deepest gratitude to my wife, İrem Bezciöglu Göktolga, for her love, assistance and understanding. Through every stage of this Master's study, whenever I become desperate, her existence has comforted me and made me go on.

TABLE OF CONTENTS

ABSTRACT	iv
ÖZ	vi
ACKNOWLEDGMENTS	ix
TABLE OF CONTENTS	x
LIST OF TABLES	xii
LIST OF FIGURES	xiii
LIST OF SYMBOLS AND ABBREVIATIONS	xv
CHAPTERS	
1. INTRODUCTION	1
1.1 LSFEM	1
1.2 Conjugate Heat Transfer	4
1.3 Outline of the Thesis	7
2. FORMULATIONS AND METHODS USED	10
2.1 General Numerical Procedure	10
2.1.1 Forced Convection Solver	10
2.1.2 Natural Convection Solver.....	11
2.2 Governing Equations	12
2.2.1 Equations for Viscous Incompressible Newtonian Flows	12
2.2.1.1 Continuity Equation	12
2.2.1.2 Conservation of Momentum Equations	12
2.2.1.3 Conservation of Energy Equation	13
2.2.2 Energy Equation for Solids.....	14
2.2.3 Natural Convection Equations	14
2.3 LSFEM Formulation	15
2.3.1 Basics of Classical Galerkin FEM formulation	15
2.3.2 Basics of LSFEM Formulation	18
2.3.3 Governing Equations in LSFEM Form.....	22
2.3.3.1 Conservation of Mass and Momentum Equations	22
2.3.3.2 Energy Equation.....	24
2.3.3.3 Natural Convection Equations	26
2.4 Used Element Types.....	29
2.5 Linear Solver and Storage Schemes	34

3. CODE VALIDATION	36
3.1 Flow Solver Validation	36
3.1.1 3D Lid Driven Cavity Flow	36
3.1.2 Backward Facing Step (BFS) Flow	40
3.2 Heat Transfer Solver Validation.....	48
3.2.1 Thermally Driven Cavity (TDC) Flow	48
3.3 Conjugate Heat Transfer Solver Validation	52
3.3.1 Conjugate Heat Transfer in Thermally Driven Cavity Flow	52
3.3.2 Conjugate Heat Transfer in Couette Flow	54
4. SIMULATION OF CONJUGATE HEAT TRANSFER IN A MICROCHANNEL	56
5. CONCLUSIONS AND DISCUSSIONS	70
REFERENCES.....	74

LIST OF TABLES

TABLES

Table 2.1 Node Numbers of Different Elements	30
Table 3.1 Values of Geometric Parameters for BFS Problem	41
Table 3.2 Flow and Fluid Properties for BFS Flow	42
Table 3.3 γ -Vorticity at the Center of the Cavity, Maximum Velocities and Their Positions along Centerlines.....	51
Table 4.1 Geometrical Dimensions of Single Channel.....	58
Table 4.2 Properties of Fluid Used in Flow Calculations	61
Table 4.3 Properties of Materials Used in Heat Transfer Calculations.....	63

LIST OF FIGURES

FIGURES

Figure 1.1 Two Adjacent Cells on Fluid-Solid Interface for a CHT Problem [36]	4
Figure 1.2 Sample Microchannel Arrangement [44]	7
Figure 2.1 Sample Piecewise Continuous Polynomial Approximation over Finite Elements [50].....	16
Figure 2.2 Elemental Shape Functions over 1D Element	21
Figure 2.3 Lagrange Type Quadrilateral Elements: (a) Linear, (b) Quadratic [52] ..	30
Figure 2.4 Triangular Elements: (a) Linear, (b) Quadratic	30
Figure 2.5 Lagrange Type Hexagonal Elements: (a) Linear, (b) Quadratic	31
Figure 2.6 Tetrahedron Elements: (a) Linear, (b) Quadratic	31
Figure 2.7 Linear Quadrilateral Master Element	33
Figure 2.8 1D Master Element and Shape Functions.....	33
Figure 3.1 Configuration for 3D Lid Driven Cavity Flow [7]	37
Figure 3.2 Non-Uniform Top Wall Mesh for 3D Lid Driven Cavity Flow	37
Figure 3.3 u - and v -velocity Contours at.....	38
Figure 3.4 Velocity Profiles along Centerlines for $Re=100$	39
Figure 3.5 Velocity Profiles along Centerlines for $Re=1000$	39
Figure 3.6 Geometric Parameters of the Backward Facing Step Flow [60]	41
Figure 3.7 Primary Circulation Region and Reattachment Length [60]	42
Figure 3.8 Surface Mesh for	43
Figure 3.9 Change of Primary Reattachment Length with Reynolds Number	44
Figure 3.10 Change of Primary Reattachment Length in z -direction at $Re=648$	45
Figure 3.11 The Points through Which u -Velocities are Compared in z	46
Figure 3.12 Change of u -Velocities along z -Direction at $x_1/S = 0$ and Different y - Stations, $Re=648$	46
Figure 3.13 Change of u -Velocities along z -Direction at $y = 7.5$ mm and at different x -Stations, $Re=648$	47
Figure 3.14 General Geometry and Boundary Conditions for TDC Flow [63].....	48
Figure 3.15 Comparison of u -Velocities along Centerline in z -Direction, $Ra=10^5$..	49
Figure 3.16 Comparison of w -Velocities along Centerline in x -Direction, $Ra=10^5$.	49
Figure 3.17 Temperature Contours for $Ra=10^6$ at $y = 0.5$, Wakashima and Saitoh [63] (left), Current Work (right)	50
Figure 3.18 General View of Thermally Driven Cavity with Conjugate Heat Transfer [38].....	52
Figure 3.19 Comparison of Temperature Contours for.....	53
Figure 3.20 Temperature Distribution along the Interface for Different K	54
Figure 3.21 General View of Couette Flow with Conjugate Heat Transfer [36].....	54

Figure 3.22 Temperature Profiles for Couette Flow in y -Direction for Different K .	55
Figure 4.1 Tested Microchannel by Kawano et al. [46].....	56
Figure 4.2 Geometry and Boundaries for Single Microchannel to be Simulated [42]	58
Figure 4.3	60
Figure 4.4 Change of Poiseuille's Constant with Reynolds Number.....	62
Figure 4.5 Change of Thermal Resistance with Reynolds Number.....	64
Figure 4.6 Change of Bulk Temperature in x -Direction.....	65
Figure 4.7 Change of Interface Temperatures in x -Direction ($y = Hy2$ Wall on Left and $z = Hz2$ Wall on Right)	66
Figure 4.8 Change of Interface Heat Fluxes into the Fluid in x -Direction ($y = Hy2$ Wall on Left and $z = Hz2$ Wall on Right).....	67

LIST OF SYMBOLS AND ABBREVIATIONS

[A]	Differential Operator Vector
[K]	Stiffness Matrix
{ B }	Boundary Integral Vector
{ F }	Force Vector
{ U }	Unknown Vector
BDIM	Boundary Domain Integral Method
BEM	Boundary Element Method
BFS	Backward Facing Step
BLAS	Basic Linear Algebra Subprogram
C	Poiseuille's Constant
C^0	Continuity of Order Zero
CHT	Conjugate Heat Transfer
c_p	Thermal Capacity
D_h	Hydraulic Diameter
e	Internal Energy
EBC	Essential Boundary Condition
EBE	Element by Element
f	Body Force Vector
f	Force Vector in FEM Formulation / Friction Factor
FDM	Finite Difference Method
FEM	Finite Element Method
FOSLL*	First Order System LL*
FOSLS	First Order System Least Squares
Fr	Froude Number
FSI	Fluid Structure Interaction
FVM	Finite Volume Method
g	Gravity Vector
GFEM	Galerkin Finite Element Method
GLS	Galerkin Least Squares
h	Enthalpy / Channel Height Before Step Channel Height After Step / Microchannel Configuration Channel
H	Height and Width Dimensions
HVAC	Heating-Ventilating-Air Conditioning
k	Thermal Conductivity
K	Thermal Conductivity Ratio
l	Channel Length Before Step
L	Channel Length After Step / Microchannel Length
LHS	Left Hand Side

LSFEM	Least Squares Finite Element Method
m	Number of Unknowns at Each Node
NBC	Natural Boundary Condition
N_{bc}	Number of Boundary Conditions
NE	Number of Elements
N_{elem}	Number of Elements
N_{eq}	Number of Differential Equations
N_{Gauss}	Number of Gauss Quadrature Points
NN	Number of Nodes
N_{node}	Number of Nodes
n_x	Unit Outward Normal
p	Pressure
Pe	Peclet Number
Pr	Prandtl Number
q	Heat Flux
$q_{interface}$	Heat Flux at Fluid-Solid Interface
$R(x)$	Residual Function
Ra	Rayleigh Number
Re	Reynolds Number
RHS	Right Hand Side
R_t	Thermal Resistance
S	Step Height
$S(x)$	Shape Function
SPD	Symmetric Positive Definite
SUPG	Streamline Upwind Petrov-Galerkin
t	Time
T	Temperature
TDC	Thermally Driven Cavity
$T_{interface}$	Temperature at Fluid-Solid Interface
u	Flow in x -Direction
u_m	Mean Velocity
\mathbf{V}	Velocity Vector
v	Flow in y -Direction
w	Flow in z -Direction
W	Channel Width / Microchannel Configuration Wall Height and Width Dimensions
$w(x)$	Weight Function
x_1	Reattachment Length
Γ	Boundary Domain
δ_{ij}	Kronecker-Delta
Δp	Pressure Drop
λ	Bulk Viscosity Coefficient
μ	Dynamic Viscosity Coefficient

ν	Kinematic Viscosity Coefficient
ρ	Density
τ	Shear Stress
Φ	Viscous Dissipation Function
Ω	Computational Domain
ω	Vorticity Vector

CHAPTER 1

INTRODUCTION

Finite Element Method (FEM) is a numerical method based on variational principles. It was first applied to structural problems in engineering with great success [1, 2]. This achievement of FEM has led engineers and mathematicians try to solve fluid flow problems with the same variational settings. Since the Navier-Stokes equations are non-self adjoint, instead of variational principles such as the minimization of total potential energy, weighted residual formulations such as Galerkin FEM was used to simulate fluid flow [3]. However, for convection dominated flows, simple application of Galerkin FEM may lead to inaccurate results. In order to overcome this problem, several modified (stabilized) versions of Galerkin FEM were introduced such as Galerkin Least Squares (GLS), Streamline Upwind Petrov-Galerkin (SUPG), etc. For the same reasons, but with a different mathematical background, Least Squares Finite Element Method (LSFEM) has also been introduced and applied to fluid flow problems [4].

1.1 LSFEM

LSFEM is based on minimization of residual in a least-squares sense. It has gained much interest in fluid flow computations in the last few decades. The reason for the growing attraction stems from its many advantages over other finite element formulations. The basic advantage of LSFEM is that the resulting stiffness matrix is symmetric and positive definite [5]. Therefore, resulting sets of equations can be solved by iterative solvers efficiently. In addition, since the stiffness matrix is sparse, sparse storage schemes can be used. Together with the use of iterative solvers instead of direct ones, memory requirement for LSFEM is very low.

Another advantage of LSFEM is its applicability to all kinds of partial differential equations (elliptic, parabolic and hyperbolic) without any major modifications [5]. On the other hand, there are many versions of finite difference or Galerkin FEM formulations depending on the problem of interest.

For convective dominant flows, Galerkin FEM causes numerical oscillations [3]. To overcome these oscillations, either some stabilization techniques are applied or excessively dense grids are used. On the other hand, LSFEM comes with a built in stabilization and does not need any special treatment [5]. Owing to this feature, LSFEM can use equal order shape functions for all variables.

In LSFEM with C^0 continuous approximations, it is first necessary to reduce the order of differential equation set to one. In order to do so, additional unknowns must be defined and then extra equations constituting relationship between additional unknowns and original ones must be written. These additional unknowns and equations bring increased computational costs and this is the main disadvantage of LSFEM. However, this disadvantage is compensable considering the resulting symmetric positive definite system. There may be different selections of additional unknowns and extra equations for a given set of differential equations. For Navier-Stokes equations, there are three well-known first order formulations. The most widely used one is the velocity-vorticity-pressure formulation [6-8]. There are also velocity-stress-pressure [5, 9] and velocity-velocity flux-pressure [10, 11] formulations. All these formulations were evaluated by Kayser-Herold and Matthies and it was concluded that none of them is superior over others mathematically as they all need some kind of modifications for optimal convergence [2]. Therefore, velocity-vorticity-pressure formulation was used in this study since it is the most widely used one and it brings minimum amount of extra unknowns and equations. It is also essential to reduce the order of energy equation to one. In many works, heat flux was introduced as the additional unknown [5, 12-14]. No alternative to this first order formulation was found for the energy equation and hence, heat flux and its definition were used as additional unknown and equations.

In addition to definition of vorticity in velocity-vorticity-pressure formulation, Jiang also added the divergence of vorticity equation to the system to satisfy the ellipticity of the equations [5]. However, Bochev showed that verification of Jiang is not completely correct but valid only under some special boundary conditions [15]. Trials with the developed code also showed that the use of divergence of vorticity equation deteriorates convergence. Therefore, for the solution of Navier-Stokes equations, additional vorticity equation was not included in the current work. Similarly, for the solution of energy equation, the use of curl of heat flux equation together with definition of heat flux was advised by Jiang [16]. Dennis and Dulikravich followed this approach and obtained satisfactory results [13]. Also in the current study, trials with and without curl of heat flux equation were conducted and better convergence rates were observed when the additional equation was used.

Since LSFEM tries to minimize the overall residual stemming from all the differential equations together, the contribution of each equation to the residual is of equal importance. As conservation of mass is represented only by the continuity equation in Stokes and Navier-Stokes equations, significance of mass conservation is underrated [2, 17]. Therefore, conservation of mass may not be satisfied for inlet-outlet type flows and this fact is another disadvantage of LSFEM. Special treatments are necessary in order to overcome the problem. Deang and Gunzburger applied a simple weighting technique via multiplying the continuity equation by a constant and obtained satisfactory results [18]. This method was also adopted in the current work due to its simplicity and effectiveness as the computations show. Alternative methods to simple weighting can be listed as setting strict boundary conditions with appropriate first order formulation and a combined FOSLS/FOSLL* approach [19, 20].

Due to the fact that the advantages of LSFEM surpass its disadvantages, it has been used to discretize many differential equation sets modeling fluid flow problems since 1970's. These equation sets and flow problems may be listed as; Stokes equations [21-23], incompressible Navier-Stokes equations [24-27], compressible Euler equations [28-30], pure convection problems [5, 31], natural convection problems [5, 12], and other flows of engineering interest [32, 33]. However, there are only a few

studies that utilized LSFEM for coupled problems where physical phenomena in fluid and solid media are analyzed together. In their fluid-structure interaction (FSI) study, Kayser-Herold and Matthies used Galerkin-FEM to model structural part and LSFEM to model fluid flow [34]. This approach causes the global algebraic system to lose its symmetric and positive definite property. In another FSI study, Heys et al. used first-order system least squares (FOSLS) to model both fluid and solid domain [35]. They used fully-coupled, semi-coupled and fully-decoupled approaches and compare the results.

In the field of conjugate heat transfer, even less work was conducted using LSFEM. This is one of the reasons why this study was devoted to developing LSFEM based solver which simulates conjugate heat transfer.

1.2 Conjugate Heat Transfer

Conjugate heat transfer (CHT) deals with modeling heat transfer in both fluid and solid regions. The most important issue in conjugate heat transfer simulations is to predict heat transfer characteristics through the fluid-solid interface. A schematic of fluid-solid interface is shown in Figure 1.1.

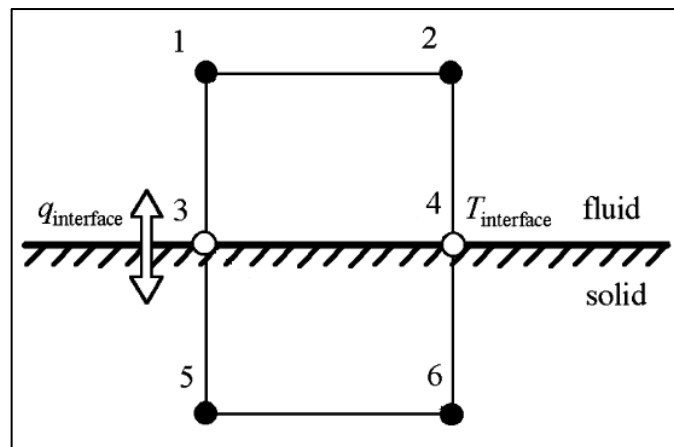


Figure 1.1 Two Adjacent Cells on Fluid-Solid Interface for a CHT Problem [36]

There are various approaches in modeling solid and fluid media and heat transfer between these two. These approaches can basically be split into two. In fully coupled approach, all the system of equations in both fluid and solid regions are formed and solved simultaneously. On the other hand, in loosely coupled approach, fluid and

solid regions are solved separately and continuity of heat flux and temperature found in each media are provided as boundary conditions to the other, and the system is solved in an iterative manner.

In [37], Patankar used finite difference method (FDM) to simulate conjugate heat transfer. He solved both the fluid and solid domain simultaneously. To assure that the velocity values were zero in solid, very high viscosity was defined for the solid region. A harmonic mean of thermal conductivities was defined between the two neighbor cells, including adjacent fluid and solid grids. Therefore, the whole system was solved at once and continuity of temperature and heat flux through the interface was ensured. Hribersek and Kuhn used boundary-domain integral method (BDIM) in [38]. They also solved flow equations in fluid and solid regions together and satisfied the zero-velocity in solid region by specifying appropriate boundary conditions along the fluid-solid interface. In addition, the continuity of heat flux and temperature was provided by defining two-way boundary conditions through the interface and hence, additional iterative procedure was avoided. On the other hand, Divo et al. [39] solved the fluid and solid parts separately, in an iterative way. They used boundary element method (BEM) to solve heat conduction equation in the solid and finite volume method (FVM) to solve compressible Navier-Stokes for the fluid region. Initially the FVM based solver worked with an adiabatic wall boundary condition and temperature output was given as boundary condition to BEM based solver. Then, steady heat conduction was solved using BEM and heat fluxes were given to fluid part as boundary condition. Iterations continued until the interface temperature and heat flux values from both solvers were close enough. Wansophark et al. used a fully coupled approach to model conjugate heat transfer [36]. They utilized streamline upwind FEM for fluid flow simulations and classical Galerkin FEM for heat conduction in solid. Triangular grids with equal order shape functions were adopted. In the only work found using LSFEM to model conjugate heat transfer, Dennis and Dulikravich simulated magneto-hydrodynamics with heat transfer in two dimensions [13]. They modeled heat transfer in both solid and fluid in a fully coupled manner. Navier-Stokes equations including energy equation for fluid and solid regions were solved together with Maxwell equations.

In the current study, fluid flow and heat transfer simulations were conducted in a separate fashion for the forced convection problems. This seems to be a valid approach when the viscous dissipation and changes of fluid properties are neglected. Therefore, the energy equation for fluid flow reduced to convection-conduction equation. As White [40] claimed, these simplifications are meaningful when the changes of velocities are low in orders of magnitude compared to heat transfer. In the flow solver, only the fluid part was modeled and the velocity values obtained were extracted to be used in the convective part of the energy equation. For the heat transfer part, a fully coupled approach to model conjugate heat transfer was adopted as Reddy [41] advised for FEM based solvers. By doing so, continuity of temperature and heat flux through the interface was automatically preserved. Velocity values for the solid part were set to zero manually and convection-conduction equation reduced to pure conduction equation, enabling the use of single energy equation for both media. The only change made to the energy equation depending on the medium was to place appropriate thermal conductivity for fluid and solid parts.

Conjugate heat transfer appears in many engineering applications such as combustion processes, HVAC systems, electronics cooling, etc. Especially in microelectronics industry, the fast growth of technology brings the need for developing more efficient and effective cooling systems. Some of the most efficient techniques in microchip cooling can be listed as; two phase flow, usage of metal foams, liquid jet impingement and microchannel heat transfer [42, 43]. Cooling with the use of microchannels is advantageous over other methods in many aspects [43]. Furthermore, they are more suitable to be simulated with the current numerical method. Therefore, solution of conjugate heat transfer phenomenon in microchannels was selected as the ultimate aim for this study. Sample microchannel geometry is presented in Figure 1.2.

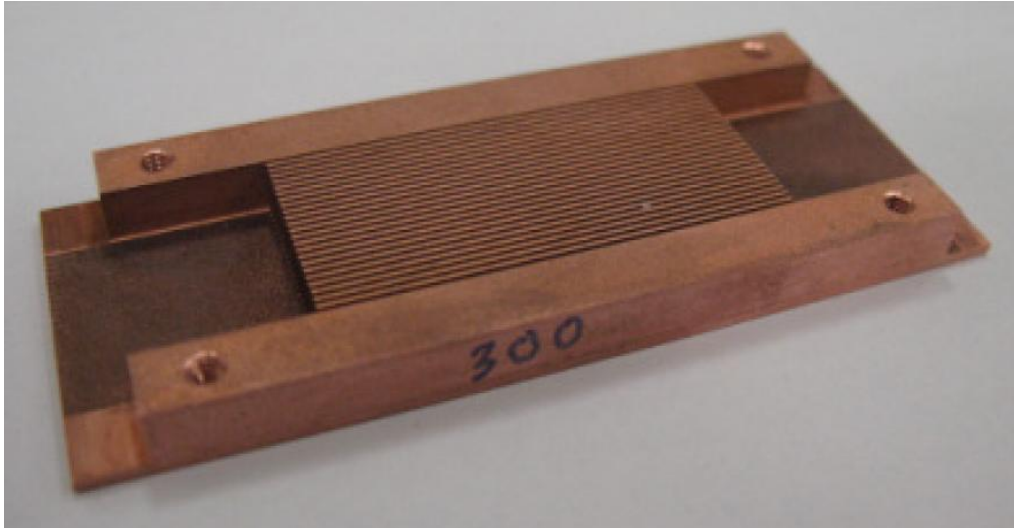


Figure 1.2 Sample Microchannel Arrangement [44]

In order to get familiar with the microchannel heat transfer concept, a literature survey covering both experimental and numerical works was conducted. In one of the pioneering works, Tuckerman [45] conducted an experimental study comparing integral cooling of electronics component and cooling through microchannels. He concluded that the use of microchannels is more appropriate considering issues like packaging, reliability and cost. Kawano et al. [46] constructed a microchannel configuration and tested it both experimentally and numerically. They also used the developed microchannels in a practical application. Fedorov and Viskanta [42] simulated the same configuration numerically for different Reynolds numbers and presented a thorough investigation of heat transfer characteristics of the system. They also made recommendations about the cooling efficiency of microchannel geometries and thermal stress related issues. Toh et al. [47] studied the effect of variable fluid properties on pressure drop characteristics. They computed the Poiseuille's constant for both constant and varied flow property cases and compared the results with Tuckerman's experimental findings. Xie et al. [48] performed optimization of water cooled minichannels with computational tools. A trade-off between the pump power and the heat removal rates was conducted and an optimum configuration was chosen.

1.3 Outline of the Thesis

Since the ultimate goal was to simulate microchannel heat transfer with the developed LSFEM based conjugate heat transfer solver, there were basic steps to

follow in this thesis research. Outline of the thesis matches with the order of these steps.

It was first necessary to extract required formulation from the literature and utilize them in code development. Therefore, the next chapter is devoted to formulations and methodologies used in the solver. Firstly, the general numerical procedure adopted in the present study is presented. Then, proper forms of governing equations of fluid flow and heat transfer phenomena are given. After brief information on FEM and in particular LSFEM formulations, first order forms of governing equations to be used in LSFEM are introduced. Finally, the element types used in the study and some other aspects of the developed code are mentioned.

The solver must be validated before its application to a microchannel problem. Validation was conducted through the simulation of well-known benchmark problems and comparison of the results with the ones in the literature. These computations and comparisons are given in Chapter 3. Initially, the flow solver was validated with two widely accepted benchmark problems, namely the lid-driven cavity and flow over backward facing step problems. Simulation of backward facing step flow was especially crucial in evaluating mass conservation issues related to LSFEM. Then, in order to evaluate the heat transfer solver, natural convection in a cubical cavity was investigated. Since the main aim is to simulate conjugate heat transfer, it is necessary to solve some benchmark problems in this field, too. However, there could not be found a widely solved conjugate heat transfer problem, especially in three dimensions. Instead, two simple two-dimensional problems investigated in some previous studies were solved.

As the code was validated through the successful simulation of abovementioned problems, solution of a microchannel heat transfer problem could be conducted. A microchannel configuration analyzed both experimentally and numerically by previous researches was found and simulated with the current code. Details of the problem and results obtained are presented in Chapter 4.

Finally, conclusions and discussions about the performance of LSFEM for conjugate heat transfer problems are given in Chapter 5. In addition, possible enhancements and future works are summarized.

CHAPTER 2

FORMULATIONS AND METHODS USED

2.1 General Numerical Procedure

In this study, there are basically two solvers. One is forced convection solver and the other one is natural convection solver. Both of them have the conjugate heat transfer capability as well. Since the aim of this work is to model a microchannel heat transfer problem, in most of the parts of the thesis the attention is given to the conjugate heat transfer solver with forced convection. Natural convection based solver was developed in order to solve the well-known and reliable benchmark problems and see the heat transfer modeling capabilities of the formulation. In here, general working principles of these two solvers are explained.

2.1.1 Forced Convection Solver

There are two basic assumptions made in the formulation of forced convection solver. The first one is that the viscous dissipation is neglected due to small changes of velocities in the flows of interest. Negligible change in fluid properties due to temperature increase is the second assumption. This is valid again for the flows solved in this study where temperature rises are small. Owing to these two simplifications, the energy equation reduces to convection-conduction equation and can be solved separately from the fluid flow part. Therefore, in forced convection solver, first the flow computations are conducted. Then, velocity values exported from the flow solver are imported to the heat transfer solver to be used in the convective part of the energy equation. Heat transfer solver is run with appropriate boundary conditions and the solution is finished.

In order to handle conjugate nature, a fully coupled approach was used as Reddy [41] suggested for FEM based codes. Zero velocity values are given to solid regions and the energy equation for solid part reduces to conduction equation. Inserting corresponding thermal conductivities for fluid and solid regions, single energy equation is solved for the whole domain. Therefore, continuity of heat flux and temperature are guaranteed and no additional thermal boundary conditions are given to the fluid-solid interface.

In the flow solver part, nonlinear convective terms appearing in momentum equations were linearized using Newton linearization. Therefore, some number of Newton linearization iterations is conducted to get converged results. To ensure convergence, velocity values from the previous iteration are compared with the current one until some specified tolerance is achieved. However, in the heat transfer solver part, no nonlinear terms are present since the velocities are no longer variables to be solved but imported values. Convergence is achieved when the error of the iterative solver drops below the specified tolerance. The details of the iterative solver is presented in the following sections.

2.1.2 Natural Convection Solver

In natural convection, fluid flow and heat transfer are coupled through Boussinesq approximation. According to the approximation, change of density is effective only in acceleration due to gravity [49]. In addition, temperature and density are related through volumetric thermal expansion. Therefore, temperature combined with gravitational acceleration appears in the momentum equations as a body force.

Since the temperature is present in flow equations, fluid flow and heat transfer are solved in a coupled manner for natural convection solver. In conjugate heat transfer problems, for solid parts, the terms related to fluid flow are equated to zero and only the energy equation is solved. In addition, for the solid regions, flow related variables (velocity, vorticity and pressure) are set to zero by defining boundary conditions.

For natural convection solver, again there are nonlinear convective terms both in momentum and energy equations. Therefore, different from the forced convection,

temperature values are also checked to observe convergence of Newton linearization steps.

2.2 Governing Equations

2.2.1 Equations for Viscous Incompressible Newtonian Flows

2.2.1.1 Continuity Equation

The continuity equation for fluid dynamics in its most general form is given below

$$\frac{D\rho}{Dt} + \rho \nabla \cdot \mathbf{V} = 0 \quad 2.1$$

where t is time, ρ is the fluid's density, \mathbf{V} is the velocity vector and D/Dt is the material derivative. For incompressible flows, the density is constant and its derivative vanishes, yielding the following continuity equation

$$\nabla \cdot \mathbf{V} = 0 \quad 2.2$$

For 3D flows in Cartesian coordinates, Eqn. (2.2) can be expanded as follows

$$\frac{\partial u}{\partial x} + \frac{\partial v}{\partial y} + \frac{\partial w}{\partial z} = 0 \quad 2.3$$

where u , v and w are the Cartesian velocity components.

2.2.1.2 Conservation of Momentum Equations

For a Newtonian fluid, conservation of momentum equations can be expressed using index notation as follows

$$\rho \frac{D\mathbf{V}}{Dt} = \rho \mathbf{f} - \nabla p + \frac{\partial}{\partial x_j} \left[\mu \left(\frac{\partial u_i}{\partial x_j} + \frac{\partial u_j}{\partial x_i} \right) + \delta_{ij} \lambda \nabla \cdot \mathbf{V} \right] = 0 \quad 2.4$$

where p is the pressure, \mathbf{f} is the body force per unit mass, μ is the dynamic viscosity and λ is the second or bulk viscosity coefficient. If the fluid is incompressible and the dynamic viscosity is constant, Eqn. (2.4) reduces to

$$\rho \frac{D\mathbf{V}}{Dt} = \rho \mathbf{f} - \nabla p + \mu \nabla^2 \mathbf{V} = \mathbf{0} \quad 2.5$$

Further assuming that the flow is steady, components of conservation of momentum equations for 3D Cartesian coordinates become

$$u \frac{\partial u}{\partial x} + v \frac{\partial u}{\partial y} + w \frac{\partial u}{\partial z} = f_x - \frac{1}{\rho} \frac{\partial p}{\partial x} + \nu \left(\frac{\partial^2 u}{\partial x^2} + \frac{\partial^2 u}{\partial y^2} + \frac{\partial^2 u}{\partial z^2} \right) \quad 2.6$$

$$u \frac{\partial v}{\partial x} + v \frac{\partial v}{\partial y} + w \frac{\partial v}{\partial z} = f_y - \frac{1}{\rho} \frac{\partial p}{\partial y} + \nu \left(\frac{\partial^2 v}{\partial x^2} + \frac{\partial^2 v}{\partial y^2} + \frac{\partial^2 v}{\partial z^2} \right) \quad 2.7$$

$$u \frac{\partial w}{\partial x} + v \frac{\partial w}{\partial y} + w \frac{\partial w}{\partial z} = f_z - \frac{1}{\rho} \frac{\partial p}{\partial z} + \nu \left(\frac{\partial^2 w}{\partial x^2} + \frac{\partial^2 w}{\partial y^2} + \frac{\partial^2 w}{\partial z^2} \right) \quad 2.8$$

Note that density was carried to right hand side of the equations and combined with the dynamic viscosity to yield kinematic viscosity, ν .

2.2.1.3 Conservation of Energy Equation

For fluid motion, one possible way of writing the energy equation is as follows

$$\rho \frac{De}{Dt} = -p \nabla \cdot \mathbf{V} + \Phi + \nabla(k \nabla T) \quad 2.9$$

where T is the temperature, Φ is the dissipation function, e is the internal energy per unit mass and k is the thermal conductivity. Defining enthalpy, $h = e + \frac{p}{\rho}$, and taking k as constant, the Eqn. (2.9) becomes

$$\rho \frac{Dh}{Dt} = \frac{Dp}{Dt} + \Phi + k \nabla^2 T \quad 2.10$$

Dissipation function is defined using index notation as

$$\Phi = \tau_{ij} \frac{\partial u_i}{\partial x_j} \quad 2.11$$

If the change of flow velocities is small in orders of magnitude compared to that of heat transfer, as is the case for the scope of this thesis, Dp/Dt and Φ can be neglected since they are both on the order of square of velocity [40]. By using this assumption and inserting $h = c_p dT$, energy equation for fluid flow becomes

$$\rho c_p \frac{DT}{Dt} = k \nabla^2 T \quad 2.12$$

This form of the energy equation can simply be called as the convection-conduction equation for fluids. Again, assuming steady flow, energy equation for fluid domain in 3D Cartesian coordinates becomes

$$\rho c_p \left(u \frac{\partial T}{\partial x} + v \frac{\partial T}{\partial y} + w \frac{\partial T}{\partial z} \right) = k \left(\frac{\partial^2 T}{\partial^2 x} + \frac{\partial^2 T}{\partial^2 y} + \frac{\partial^2 T}{\partial^2 z} \right) \quad 2.13$$

2.2.2 Energy Equation for Solids

Neglecting heat generation, steady-state energy equation for solids is simply the following conduction equation

$$k \left(\frac{\partial^2 T}{\partial^2 x} + \frac{\partial^2 T}{\partial^2 y} + \frac{\partial^2 T}{\partial^2 z} \right) = 0 \quad 2.14$$

As can easily be deduced from Eqn. (2.13) and (2.14), convection-conduction equation can be solved for both fluid and solid parts by setting velocity values for solid to zero and using appropriate thermal conduction coefficients.

2.2.3 Natural Convection Equations

To test the LSFE formulation's ability for simulation of heat transfer in incompressible flows, a natural convection solver was developed in addition to the main code. Following dimensionless equations were taken from Tang and Tsang [12]

$$\nabla \cdot \mathbf{V} = 0 \quad 2.15$$

$$\frac{\partial \mathbf{V}}{\partial t} + \mathbf{V} \cdot \nabla \mathbf{V} + \nabla p - \frac{1}{Re} \nabla^2 \mathbf{V} + \frac{1}{Fr} \mathbf{g} T = 0 \quad 2.16$$

$$\frac{\partial T}{\partial t} + \mathbf{V} \cdot \nabla T - \frac{1}{Pe} \nabla^2 T = 0 \quad 2.17$$

where \mathbf{g} is the gravity vector, and the dimensionless numbers are defined as

$$Pr = \frac{c_p \mu}{k} = \frac{\nu}{\alpha}$$

$$Fr = \frac{U^2}{\gamma \Delta T g D}$$

$$Ra = \frac{\gamma g D^3 \Delta T}{\alpha \nu}$$

$$Re = \sqrt{\frac{Ra}{Pr}}$$

$$Pe = \sqrt{Ra Pr}$$

For steady flow in 3D Cartesian coordinates, assuming the gravity is in negative z-direction, the equations take the following form

$$\frac{\partial u}{\partial x} + \frac{\partial v}{\partial y} + \frac{\partial w}{\partial z} = 0 \quad 2.18$$

$$u \frac{\partial u}{\partial x} + v \frac{\partial u}{\partial y} + w \frac{\partial u}{\partial z} + \frac{\partial p}{\partial x} - \frac{1}{Re} \left(\frac{\partial^2 u}{\partial x^2} + \frac{\partial^2 u}{\partial y^2} + \frac{\partial^2 u}{\partial z^2} \right) = 0 \quad 2.19$$

$$u \frac{\partial v}{\partial x} + v \frac{\partial v}{\partial y} + w \frac{\partial v}{\partial z} + \frac{\partial p}{\partial y} - \frac{1}{Re} \left(\frac{\partial^2 v}{\partial x^2} + \frac{\partial^2 v}{\partial y^2} + \frac{\partial^2 v}{\partial z^2} \right) = 0 \quad 2.20$$

$$u \frac{\partial w}{\partial x} + v \frac{\partial w}{\partial y} + w \frac{\partial w}{\partial z} + \frac{\partial p}{\partial z} - \frac{1}{Re} \left(\frac{\partial^2 w}{\partial x^2} + \frac{\partial^2 w}{\partial y^2} + \frac{\partial^2 w}{\partial z^2} \right) - \frac{1}{Fr} T = 0 \quad 2.21$$

$$\left(u \frac{\partial T}{\partial x} + v \frac{\partial T}{\partial y} + w \frac{\partial T}{\partial z} \right) - \frac{1}{Pe} \left(\frac{\partial^2 T}{\partial x^2} + \frac{\partial^2 T}{\partial y^2} + \frac{\partial^2 T}{\partial z^2} \right) = 0 \quad 2.22$$

2.3 LSFEM Formulation

2.3.1 Basics of Classical Galerkin FEM formulation

In order to explain the basic steps in a finite element analysis, the following sample differential equation that represents 1D, steady advection-diffusion phenomena is used

$$u \frac{dT}{dx} - k \frac{d^2T}{dx^2} = f \quad 2.23$$

This equation can be solved by approximating it on finite elements, which are obtained by discretizing the domain. Discretization and polynomial approximation procedure on a domain composed of NE finite elements can be seen in Figure 2.1.

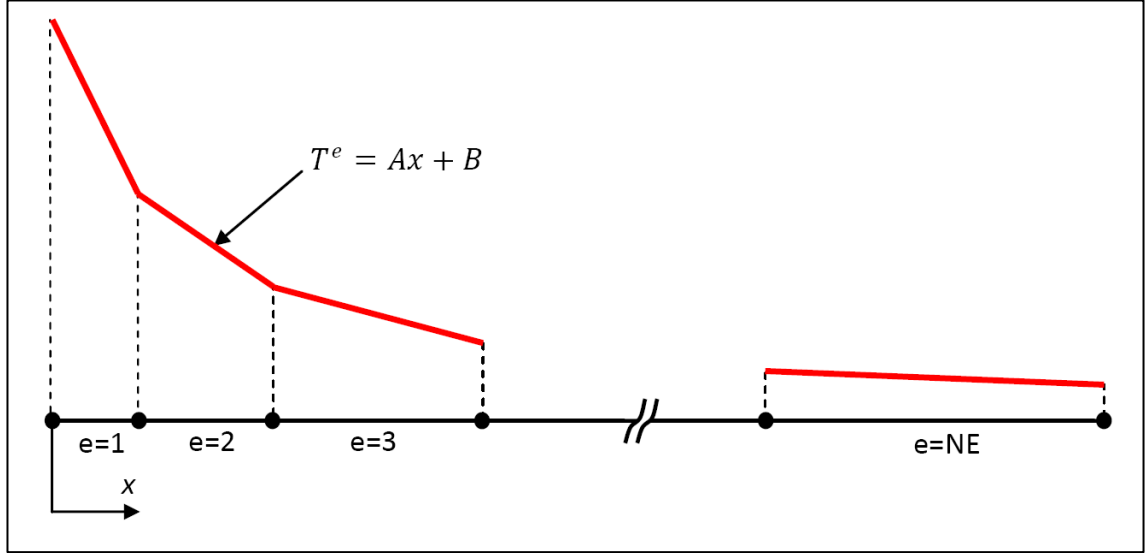


Figure 2.1 Sample Piecewise Continuous Polynomial Approximation over Finite Elements [50]

As can be seen from Figure 2.1, the approximations over the elements are linear. The overall solution is C^0 continuous, i.e. the solution itself is continuous at element interfaces, but not its first derivative.

Considering FEM as a weighted residual type numerical method, it is possible to start the formulation with writing the following residual of the differential equation

$$R(x) = u \frac{dT}{dx} - k \frac{d^2T}{dx^2} - f \quad 2.24$$

Residual should be minimized as much as possible in order to get accurate results. In weighted residual type numerical methods, this minimization is performed in the following weighted integral sense

$$\int_{\Omega} w(x) R(x) dx = 0 \quad 2.25$$

$$\int_{\Omega} \left(wu \frac{dT}{dx} - wk \frac{d^2T}{dx^2} - wf \right) dx = 0 \quad 2.26$$

Here Ω represents the computational domain. Since the differential equation is second order and approximations over elements are only first order, the term with second order derivative needs special care. For most of the finite element methods, integration by parts is applied to second order derivatives

$$\int_{\Omega} -wk \frac{d^2T}{dx^2} dx = \int_{\Omega} k \frac{dw}{dx} \frac{dT}{dx} dx - \int_{\Gamma} wk \frac{dT}{dx} n_x d\Gamma \quad 2.27$$

where Γ represents the boundary of the domain with its unit outward normal being n_x . Substituting Eqn. (2.27) into (2.26), the following expression is obtained

$$\int_{\Omega} \left(wu \frac{dT}{dx} + k \frac{dw}{dx} \frac{dT}{dx} \right) dx = \int_{\Omega} wf dx + \int_{\Gamma} \underbrace{wk \frac{dT}{dx} n_x}_{q_n} d\Gamma \quad 2.28$$

Note that the second term on RHS includes $k \frac{dT}{dx}$, which is equal to heat flux with a minus sign in front. Heat flux is a kind of natural (or Neumann) boundary condition (NBC) and automatic inclusion of NBC in the system is an advantage of FEM. The next step is to write the equations in terms of approximations over nodes.

$$T^h(x) = \sum_{j=1}^{NN} T_j S_j \quad 2.29$$

where T^h is the approximate solution that is chased, NN is the number of nodes in the domain, T_j 's are the nodal unknowns and S_j 's are the user selected shape functions. Putting this equation into the weighted residual statement, one gets

$$\int_{\Omega} \left[wu \left(\sum T_j \frac{dS_j}{dx} \right) + k \frac{dw}{dx} \left(\sum T_j \frac{dS_j}{dx} \right) \right] dx = \int_{\Omega} wf dx - \int_{\Gamma} w q_n d\Gamma \quad 2.30$$

One of the most important aspects in an FEM is the selection of weight functions. In Galerkin FEM, the weight functions are selected to be the same as shape functions. Since there are NN shape functions, there are NN different selections for weight function and this leads to NN different equations that can be used to solve for NN nodal unknowns. It is possible to represent these set of equations in matrix form as

$$[K]\{U\} = \{F\} + \{B\} \quad 2.31$$

where $[K]$ is the stiffness matrix, $\{U\}$ is the nodal unknown vector, $\{F\}$ is the force vector and $\{B\}$ is the so called boundary integral vector, given as follows

$$K_{ij} = \int_{\Omega} \left(S_i u \frac{dS_j}{dx} + k \frac{dS_i}{dx} \frac{dS_j}{dx} \right) dx \quad F_i = \int_{\Omega} S_i f dx \quad B_i = \int_{\Gamma} S_i q_n d\Gamma \quad 2.32$$

Values of NN nodal unknowns are found by solving this system of equations. In order to implement this procedure into a computer code, integrals in Eqn. (2.32) are written and evaluated separately for each element instead of the whole domain. Then the global system is formed by assembling elemental ones.

2.3.2 Basics of LSFEM Formulation

If the elements with more continuity than C^0 are used with LSFEM, it becomes almost impossible to construct residual equations, especially in 3D [2]. Furthermore, LSFEM is applicable to first order differential equations when C^0 continuous elements are used. Therefore, it is a prerequisite to decrease the order of differential equation to one. This is accomplished by defining new variables and adding extra differential equations. For Eqn. (2.23), definition of the following flux is appropriate

$$q = -k \frac{dT}{dx} \quad 2.33$$

using which 1D steady advection-diffusion equation can be written as follows

$$u \frac{dT}{dx} + \frac{dq}{dx} = f \quad 2.34$$

Now the heat flux appears as an unknown. Therefore, instead of specifying the derivative of temperature as NBC, heat flux is specified as essential (or Dirichlet) boundary condition (EBC). Since the derivatives of the unknowns in the original differential equations are defined as new variables in LSFEM, always the EBC's are defined on the boundaries. This is a unique property of LSFEM.

There are two first order differential equations now; Eqn. (2.33) and (2.34), which can be written in matrix form as follows

$$\begin{bmatrix} u \frac{d}{dx} & \frac{d}{dx} \\ k \frac{d}{dx} & 1 \end{bmatrix} \begin{Bmatrix} T \\ q \end{Bmatrix} = \begin{Bmatrix} f \\ 0 \end{Bmatrix} \quad 2.35$$

or in a compact form as

$$[A]\{U\} = \{F\} \quad 2.36$$

where $[A]$ is the differential operator matrix, $\{U\}$ is the unknown vector and $\{F\}$ is the RHS vector. The weighted residual form of these two equations are written as follows

$$\int_{\Omega} w^1 \underbrace{\left(u \frac{dT}{dx} + \frac{dq}{dx} - f \right)}_{R^1} dx = 0 \quad 2.37$$

$$\int_{\Omega} w^2 \underbrace{\left(k \frac{dT}{dx} + q \right)}_{R^2} dx = 0 \quad 2.38$$

where w^1 and w^2 are the weight functions, R^1 and R^2 are residuals of the first and second differential equation respectively.

Approximate solution for LSFEM has the same form as Galerkin FEM, given by Eqn. (2.29). But in addition to T , the second unknown q also needs to be discretized in a similar way

$$q^h(x) = \sum_{j=1}^{NN} q_j S_j \quad 2.39$$

Unlike Galerkin FEM, in LSFEM weight functions are selected to be the derivatives of the residuals with respect to nodal unknowns, which mathematically corresponds to the minimization of residual in a least squares sense. To explain the details further, it is better to write the contribution to the residual of only one node, say, 1st node of the domain.

$$R_1^1 = u T_1 \frac{dS_1}{dx} + q_1 \frac{dS_1}{dx} - f_1 \quad 2.40$$

$$R_1^2 = kT_1 \frac{dS_1}{dx} + q_1 S_1 \quad 2.41$$

The superscripts of residual represent the equation number, whereas subscripts are for node number. Since the weight functions are derivatives of nodal unknowns, they can be written as

$$w_{11}^1 = \frac{\partial R_1^1}{\partial T_1} = \frac{\partial}{\partial T_1} \left(u \sum_{j=1}^{NN} T_j \frac{dS_j}{dx} + \sum_{j=1}^{NN} q_j \frac{dS_j}{dx} - f \right) = u \frac{dS_1}{dx} \quad 2.42$$

where first subscript of weight function represents node number and the second subscript represents unknown number, i.e., T or q . Other weight functions can be written similarly

$$w_{12}^1 = \frac{\partial R_1^1}{\partial q_1} = \frac{dS_1}{dx} \quad 2.43$$

$$w_{11}^2 = \frac{\partial R_1^2}{\partial T_1} = k \frac{dS_1}{dx} \quad 2.44$$

$$w_{12}^2 = \frac{\partial R_1^2}{\partial q_1} = S_1 \quad 2.45$$

Using differential operator matrix and unknown vector, residual equations can be written in compact form as

$$[R_1] = [A][S_1]\{U_1\} - \{F_1\} \quad 2.46$$

where $[S_1]$ is a 2x2 matrix of which the diagonal elements are S_1 (shape function of the first node) and other elements are zero. Similarly, weight functions can be written in matrix form as

$$[w_1] = [A][S_1] \quad 2.47$$

As stated earlier, for computer implementation purposes, weighted residual equations are written for each element and then assembled to solve global equations. Consider the one dimensional element and shape functions over it, shown in Figure 2.2

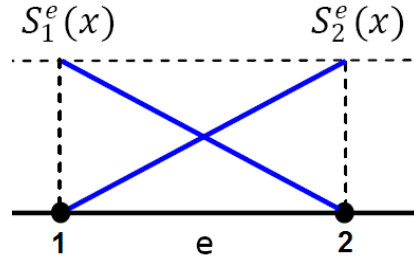


Figure 2.2 Elemental Shape Functions over 1D Element

where 1 and 2 are elemental node numbers, not the global. Writing Eqn. (2.37) and (2.38) for both of the nodes of the one dimensional element and inserting Eqn. (2.46) and (2.47), elemental stiffness matrix and force vector can be written again in compact form without the matrix brackets

$$K^e = \int_{\Omega_e} (AS^e)^T (AS^e) dx \quad F^e = \int_{\Omega_e} f (AS^e) dx \quad 2.48$$

where superscript T represents transpose and S^e is elemental shape function matrix and defined as

$$S^e = \begin{bmatrix} S_1^e & 0 & S_2^e & 0 \\ 0 & S_1^e & 0 & S_2^e \end{bmatrix} \quad 2.49$$

As can be deduced from Equation 2.48, elemental stiffness matrix is symmetric. This is one of the most important features of LSFEM. Furthermore, it is also a crucial advantage that after developing a solver for a differential equation set using the relations explained above, one almost only needs to change the differential equation operator $[A]$ to adapt the code for other kinds of differential equation sets. However, it should be mentioned that the 1D advection-diffusion equation is an ordinary differential equation. As Jiang proposes in [5], for a partial differential equation set in 3D, it is more appropriate to write the differential operator and equations in the following form

$$[A_0]\{U\} + [A_1] \frac{\partial \{U\}}{\partial x} + [A_2] \frac{\partial \{U\}}{\partial y} + [A_3] \frac{\partial \{U\}}{\partial z} = \{F\} \quad 2.50$$

The differential operator matrices will be given for each type of modeled problem in the Section 2.3.3.

It should also be noted that in a computer implementation, integrals in Eqn. (2.48) should be evaluated numerically. In FEM based solvers, mostly the Gauss quadrature is used as numerical integration scheme.

2.3.3 Governing Equations in LSFEM Form

2.3.3.1 Conservation of Mass and Momentum Equations

As explained in Chapter 1, velocity-vorticity-pressure formulation was used to make Navier-Stokes equations first order. In this formulation, vorticity is defined as an additional unknown and second order derivatives of velocities in momentum equations are rewritten in terms of vorticity. This brings one extra unknown for 2D and three extra unknowns for 3D problems. In addition, definition of vorticity components, given below, must be added as extra equations.

$$\omega_x + \frac{\partial v}{\partial z} - \frac{\partial w}{\partial y} = 0 \quad 2.51$$

$$\omega_y + \frac{\partial w}{\partial x} - \frac{\partial u}{\partial z} = 0 \quad 2.52$$

$$\omega_z + \frac{\partial u}{\partial y} - \frac{\partial v}{\partial x} = 0 \quad 2.53$$

Using these relations, Eqn. (2.6 - 2.8) can be written as follows

$$u \frac{\partial u}{\partial x} + v \frac{\partial u}{\partial y} + w \frac{\partial u}{\partial z} + \frac{1}{\rho} \frac{\partial p}{\partial x} + v \left(\frac{\partial \omega_z}{\partial y} - \frac{\partial \omega_y}{\partial z} \right) = f_x \quad 2.54$$

$$u \frac{\partial v}{\partial x} + v \frac{\partial v}{\partial y} + w \frac{\partial v}{\partial z} + \frac{1}{\rho} \frac{\partial p}{\partial y} + v \left(\frac{\partial \omega_x}{\partial z} - \frac{\partial \omega_z}{\partial x} \right) = f_y \quad 2.55$$

$$u \frac{\partial w}{\partial x} + v \frac{\partial w}{\partial y} + w \frac{\partial w}{\partial z} + \frac{1}{\rho} \frac{\partial p}{\partial z} + v \left(\frac{\partial \omega_y}{\partial x} - \frac{\partial \omega_x}{\partial y} \right) = f_z \quad 2.56$$

With continuity equation staying the same, there are 7 equations for 7 unknowns. Here it is important to note that the extra equation for the divergence of vorticity, proposed by Jiang [5], was not used in the current study.

There is one more issue to solve before the stiffness matrices can be formed; the nonlinear convective terms in conservation of momentum equations. These nonlinear

terms must be linearized in some way to solve Navier-Stokes equations. There are basically two types of popular linearization techniques being Newton linearization and successive substitution. Successive substitution is more stable whereas Newton linearization provides faster convergence. Due to this quick convergence and ability to converge when used with appropriate initial guesses, Newton linearization was preferred in this study. Newton linearization is performed as follows

$$u \frac{\partial u}{\partial x} = u_0 \frac{\partial u}{\partial x} + u \frac{\partial u_0}{\partial x} - u_0 \frac{\partial u_0}{\partial x} \quad 2.57$$

where u_0 is the velocity value from previous iteration or initial guess. As u_0 approaches u , i.e. the solution converges, left and right hand sides of Eqn. (2.57) become equal. After Newton linearization; the unknown vector, resulting coefficient matrices and force vector become

$$\mathbf{U} = \begin{bmatrix} u \\ v \\ w \\ \omega_x \\ \omega_y \\ \omega_z \\ p \end{bmatrix} \quad 2.58$$

$$A_0 = \begin{bmatrix} 0 & 0 & 0 & 0 & 0 & 0 & 0 \\ \frac{\partial u_0}{\partial x} & \frac{\partial u_0}{\partial y} & \frac{\partial u_0}{\partial z} & 0 & 0 & 0 & 0 \\ \frac{\partial v_0}{\partial x} & \frac{\partial v_0}{\partial y} & \frac{\partial v_0}{\partial z} & 0 & 0 & 0 & 0 \\ \frac{\partial w_0}{\partial x} & \frac{\partial w_0}{\partial y} & \frac{\partial w_0}{\partial z} & 0 & 0 & 0 & 0 \\ 0 & 0 & 0 & -1 & 0 & 0 & 0 \\ 0 & 0 & 0 & 0 & -1 & 0 & 0 \\ 0 & 0 & 0 & 0 & 0 & -1 & 0 \end{bmatrix} \quad 2.59$$

$$A_1 = \begin{bmatrix} 1 & 0 & 0 & 0 & 0 & 0 & 0 \\ u_0 & 0 & 0 & 0 & 0 & 0 & 1/\rho \\ 0 & u_0 & 0 & 0 & 0 & -v & 0 \\ 0 & 0 & u_0 & 0 & v & 0 & 0 \\ 0 & 0 & 0 & 0 & 0 & 0 & 0 \\ 0 & 0 & -1 & 0 & 0 & 0 & 0 \\ 0 & 1 & 0 & 0 & 0 & 0 & 0 \end{bmatrix} \quad 2.60$$

$$A_2 = \begin{bmatrix} 0 & 1 & 0 & 0 & 0 & 0 & 0 \\ v_0 & 0 & 0 & 0 & 0 & v & 0 \\ 0 & v_0 & 0 & 0 & 0 & 0 & 1/\rho \\ 0 & 0 & v_0 & -v & 0 & 0 & 0 \\ 0 & 0 & 1 & 0 & 0 & 0 & 0 \\ 0 & 0 & 0 & 0 & 0 & 0 & 0 \\ -1 & 0 & 0 & 0 & 0 & 0 & 0 \end{bmatrix} \quad 2.61$$

$$A_3 = \begin{bmatrix} 0 & 0 & 1 & 0 & 0 & 0 & 0 \\ w_0 & 0 & 0 & 0 & -v & 0 & 0 \\ 0 & w_0 & 0 & v & 0 & 0 & 0 \\ 0 & 0 & w_0 & 0 & 0 & 0 & 1/\rho \\ 0 & -1 & 0 & 0 & 0 & 0 & 0 \\ 1 & 0 & 0 & 0 & 0 & 0 & 0 \\ 0 & 0 & 0 & 0 & 0 & 0 & 0 \end{bmatrix} \quad 2.62$$

$$\mathbf{f} = \begin{bmatrix} 0 \\ f_x + u_0 \frac{\partial u_0}{\partial x} + v_0 \frac{\partial u_0}{\partial y} + w_0 \frac{\partial u_0}{\partial z} \\ f_y + u_0 \frac{\partial v_0}{\partial x} + v_0 \frac{\partial v_0}{\partial y} + w_0 \frac{\partial v_0}{\partial z} \\ f_z + u_0 \frac{\partial w_0}{\partial x} + v_0 \frac{\partial w_0}{\partial y} + w_0 \frac{\partial w_0}{\partial z} \\ 0 \\ 0 \\ 0 \end{bmatrix} \quad 2.63$$

2.3.3.2 Energy Equation

For energy equation, it is necessary to reduce the order of differentiation of temperature. In many works, heat flux was introduced [5, 12-14] as the additional unknown. The first order formulization of energy equation for 3D Cartesian coordinates become

$$\rho c_p \left(u \frac{\partial T}{\partial x} + v \frac{\partial T}{\partial y} + w \frac{\partial T}{\partial z} \right) + \frac{\partial q_x}{\partial x} + \frac{\partial q_y}{\partial y} + \frac{\partial q_z}{\partial z} = 0 \quad 2.64$$

$$q_x + k \frac{\partial T}{\partial x} = 0 \quad 2.65$$

$$q_y + k \frac{\partial T}{\partial y} = 0 \quad 2.66$$

$$q_z + k \frac{\partial T}{\partial z} = 0 \quad 2.67$$

Curl of heat flux equations were added to the system as mentioned in Chapter 1.

$$\frac{\partial q_z}{\partial y} - \frac{\partial q_y}{\partial z} = 0 \quad 2.68$$

$$\frac{\partial q_x}{\partial z} - \frac{\partial q_z}{\partial x} = 0 \quad 2.69$$

$$\frac{\partial q_y}{\partial x} - \frac{\partial q_x}{\partial y} = 0 \quad 2.70$$

Since heat transfer solver works in an uncoupled manner with the flow solver, velocity values do not change during heat transfer solution. Therefore, there is no nonlinear term in the equation set. The resulting unknown vector and coefficient matrices become

$$\mathbf{U} = \begin{bmatrix} T \\ q_x \\ q_y \\ q_z \end{bmatrix} \quad 2.71$$

$$A_0 = \begin{bmatrix} 0 & 0 & 0 & 0 \\ 0 & 1 & 0 & 0 \\ 0 & 0 & 1 & 0 \\ 0 & 0 & 0 & 1 \\ 0 & 0 & 0 & 0 \\ 0 & 0 & 0 & 0 \\ 0 & 0 & 0 & 0 \end{bmatrix} \quad 2.72$$

$$A_1 = \begin{bmatrix} u\rho c_p & 1 & 0 & 0 \\ k & 0 & 0 & 0 \\ 0 & 0 & 0 & 0 \\ 0 & 0 & 0 & 0 \\ 0 & 0 & 0 & 0 \\ 0 & 0 & 0 & -1 \\ 0 & 0 & 1 & 0 \end{bmatrix} \quad 2.73$$

$$A_2 = \begin{bmatrix} v\rho c_p & 0 & 1 & 0 \\ 0 & 0 & 0 & 0 \\ k & 0 & 0 & 0 \\ 0 & 0 & 0 & 0 \\ 0 & 0 & 0 & 1 \\ 0 & 0 & 0 & 0 \\ 0 & -1 & 0 & 0 \end{bmatrix} \quad 2.74$$

$$A_3 = \begin{bmatrix} w\rho c_p & 0 & 0 & 1 \\ 0 & 0 & 0 & 0 \\ 0 & 0 & 0 & 0 \\ k & 0 & 0 & 0 \\ 0 & 0 & -1 & 0 \\ 0 & 1 & 0 & 0 \\ 0 & 0 & 0 & 0 \end{bmatrix} \quad 2.75$$

The force vector is simply a null vector of size 7. Note that when the velocity values in Eqn. (2.73-2.75) are zero, the energy equation becomes heat conduction equation.

In numerical computations, both the system of equations with and without the curl of heat flux equation were tried and it was observed that the system with extra equations converge more rapidly.

2.3.3.3 Natural Convection Equations

In order to discretize the natural convection equations, the formulation proposed by Tang and Tsang was followed [12]. Vorticity and heat flux were added to the system as additional unknowns to make the system first order. The resulting system of equations in 3D Cartesian coordinates is

$$u \frac{\partial u}{\partial x} + v \frac{\partial u}{\partial y} + w \frac{\partial u}{\partial z} + \frac{\partial p}{\partial x} + \frac{1}{Re} \left(\frac{\partial \omega_z}{\partial y} - \frac{\partial \omega_y}{\partial z} \right) = 0 \quad 2.76$$

$$u \frac{\partial v}{\partial x} + v \frac{\partial v}{\partial y} + w \frac{\partial v}{\partial z} + \frac{\partial p}{\partial y} + \frac{1}{Re} \left(\frac{\partial \omega_x}{\partial z} - \frac{\partial \omega_z}{\partial x} \right) = 0 \quad 2.77$$

$$u \frac{\partial w}{\partial x} + v \frac{\partial w}{\partial y} + w \frac{\partial w}{\partial z} + \frac{\partial p}{\partial z} + \frac{1}{Re} \left(\frac{\partial \omega_y}{\partial x} - \frac{\partial \omega_x}{\partial y} \right) - \frac{1}{Fr} T = 0 \quad 2.78$$

$$\frac{\partial u}{\partial x} + \frac{\partial v}{\partial y} + \frac{\partial w}{\partial z} = 0 \quad 2.79$$

$$\omega_z + \frac{\partial u}{\partial y} - \frac{\partial v}{\partial x} = 0 \quad 2.80$$

$$\omega_x + \frac{\partial v}{\partial z} - \frac{\partial w}{\partial y} = 0 \quad 2.81$$

$$\omega_y + \frac{\partial w}{\partial x} - \frac{\partial u}{\partial z} = 0 \quad 2.82$$

$$u \frac{\partial T}{\partial x} + v \frac{\partial T}{\partial y} + w \frac{\partial T}{\partial z} + \frac{\partial q_x}{\partial x} + \frac{\partial q_y}{\partial y} + \frac{\partial q_z}{\partial z} = 0 \quad 2.83$$

$$q_x + \frac{1}{Pe} \frac{\partial T}{\partial x} = 0 \quad 2.84$$

$$q_y + \frac{1}{Pe} \frac{\partial T}{\partial y} = 0 \quad 2.85$$

$$q_z + \frac{1}{Pe} \frac{\partial T}{\partial z} = 0 \quad 2.86$$

The system is determined with 11 unknowns and 11 equations in total. Neither the divergence of vorticity nor the curl of heat flux equation was added to the system. Since the heat transfer and the flow solver work coupled for natural convection problems, the convective terms in Eqn. (2.76-2.78) and Eqn. (2.83) are the sources of nonlinearity, which were linearized through Newton linearization. The resulting unknown vector, coefficient matrices and force vector are as follows

$$\mathbf{U} = \begin{bmatrix} u \\ v \\ w \\ p \\ \omega_x \\ \omega_y \\ \omega_z \\ T \\ q_x \\ q_y \\ q_z \end{bmatrix} \quad 2.87$$

$$A_0 = \begin{bmatrix} \frac{\partial u_0}{\partial x} & \frac{\partial u_0}{\partial y} & \frac{\partial u_0}{\partial z} & 0 & 0 & 0 & 0 & 0 & 0 & 0 & 0 \\ \frac{\partial v_0}{\partial x} & \frac{\partial v_0}{\partial y} & \frac{\partial v_0}{\partial z} & 0 & 0 & 0 & 0 & 0 & 0 & 0 & 0 \\ \frac{\partial w_0}{\partial x} & \frac{\partial w_0}{\partial y} & \frac{\partial w_0}{\partial z} & 0 & 0 & 0 & 0 & -1/Fr & 0 & 0 & 0 \\ 0 & 0 & 0 & 0 & 0 & 0 & 0 & 0 & 0 & 0 & 0 \\ 0 & 0 & 0 & 0 & 1 & 0 & 0 & 0 & 0 & 0 & 0 \\ 0 & 0 & 0 & 0 & 0 & 1 & 0 & 0 & 0 & 0 & 0 \\ 0 & 0 & 0 & 0 & 0 & 0 & 1 & 0 & 0 & 0 & 0 \\ \frac{\partial T_0}{\partial x} & \frac{\partial T_0}{\partial y} & \frac{\partial T_0}{\partial z} & 0 & 0 & 0 & 0 & 0 & 0 & 0 & 0 \\ 0 & 0 & 0 & 0 & 0 & 0 & 0 & 0 & 1 & 0 & 0 \\ 0 & 0 & 0 & 0 & 0 & 0 & 0 & 0 & 0 & 1 & 0 \\ 0 & 0 & 0 & 0 & 0 & 0 & 0 & 0 & 0 & 0 & 1 \end{bmatrix} \quad 2.88$$

$$A_1 = \begin{bmatrix} u_0 & 0 & 0 & 1 & 0 & 0 & 0 & 0 & 0 & 0 & 0 \\ 0 & u_0 & 0 & 0 & 0 & 0 & -1/Re & 0 & 0 & 0 & 0 \\ 0 & 0 & u_0 & 0 & 0 & 1/Re & 0 & 0 & 0 & 0 & 0 \\ 1 & 0 & 0 & 0 & 0 & 0 & 0 & 0 & 0 & 0 & 0 \\ 0 & 0 & 0 & 0 & 0 & 0 & 0 & 0 & 0 & 0 & 0 \\ 0 & 0 & 1 & 0 & 0 & 0 & 0 & 0 & 0 & 0 & 0 \\ 0 & -1 & 0 & 0 & 0 & 0 & 0 & 0 & 0 & 0 & 0 \\ 0 & 0 & 0 & 0 & 0 & 0 & 0 & u_0 & 1 & 0 & 0 \\ 0 & 0 & 0 & 0 & 0 & 0 & 0 & 1/Pe & 0 & 0 & 0 \\ 0 & 0 & 0 & 0 & 0 & 0 & 0 & 0 & 0 & 0 & 0 \\ 0 & 0 & 0 & 0 & 0 & 0 & 0 & 0 & 0 & 0 & 0 \end{bmatrix} \quad 2.89$$

$$A_2 = \begin{bmatrix} v_0 & 0 & 0 & 0 & 0 & 0 & 1/Re & 0 & 0 & 0 & 0 \\ 0 & v_0 & 0 & 1 & 0 & 0 & 0 & 0 & 0 & 0 & 0 \\ 0 & 0 & v_0 & 0 & -1/Re & 0 & 0 & 0 & 0 & 0 & 0 \\ 0 & 1 & 0 & 0 & 0 & 0 & 0 & 0 & 0 & 0 & 0 \\ 0 & 0 & -1 & 0 & 0 & 0 & 0 & 0 & 0 & 0 & 0 \\ 0 & 0 & 0 & 0 & 0 & 0 & 0 & 0 & 0 & 0 & 0 \\ 1 & 0 & 0 & 0 & 0 & 0 & 0 & 0 & 0 & 0 & 0 \\ 0 & 0 & 0 & 0 & 0 & 0 & 0 & v_0 & 0 & 1 & 0 \\ 0 & 0 & 0 & 0 & 0 & 0 & 0 & 0 & 0 & 0 & 0 \\ 0 & 0 & 0 & 0 & 0 & 0 & 0 & 1/Pe & 0 & 0 & 0 \\ 0 & 0 & 0 & 0 & 0 & 0 & 0 & 0 & 0 & 0 & 0 \end{bmatrix} \quad 2.90$$

$$A_3 = \begin{bmatrix} w_0 & 0 & 0 & 0 & 0 & -1/Re & 0 & 0 & 0 & 0 & 0 \\ 0 & w_0 & 0 & 0 & 1/Re & 0 & 0 & 0 & 0 & 0 & 0 \\ 0 & 0 & w_0 & 1 & 0 & 0 & 0 & 0 & 0 & 0 & 0 \\ 0 & 0 & 1 & 0 & 0 & 0 & 0 & 0 & 0 & 0 & 0 \\ 0 & 1 & 0 & 0 & 0 & 0 & 0 & 0 & 0 & 0 & 0 \\ -1 & 0 & 0 & 0 & 0 & 0 & 0 & 0 & 0 & 0 & 0 \\ 0 & 0 & 0 & 0 & 0 & 0 & 0 & 0 & 0 & 0 & 0 \\ 0 & 0 & 0 & 0 & 0 & 0 & 0 & w_0 & 0 & 0 & 1 \\ 0 & 0 & 0 & 0 & 0 & 0 & 0 & 0 & 0 & 0 & 0 \\ 0 & 0 & 0 & 0 & 0 & 0 & 0 & 0 & 0 & 0 & 0 \\ 0 & 0 & 0 & 0 & 0 & 0 & 0 & 0 & 1/Pe & 0 & 0 \end{bmatrix} \quad 2.91$$

$$f = \begin{bmatrix} u_0 \frac{\partial u_0}{\partial x} + v_0 \frac{\partial u_0}{\partial y} + w_0 \frac{\partial u_0}{\partial z} \\ u_0 \frac{\partial v_0}{\partial x} + v_0 \frac{\partial v_0}{\partial y} + w_0 \frac{\partial v_0}{\partial z} \\ u_0 \frac{\partial w_0}{\partial x} + v_0 \frac{\partial w_0}{\partial y} + w_0 \frac{\partial w_0}{\partial z} \\ 0 \\ 0 \\ 0 \\ 0 \\ u_0 \frac{\partial T_0}{\partial x} + v_0 \frac{\partial T_0}{\partial y} + w_0 \frac{\partial T_0}{\partial z} \\ 0 \\ 0 \\ 0 \end{bmatrix} \quad 2.92$$

2.4 Used Element Types

For 2D problems basically two element types, triangular and quadrilateral, are used. Similarly, in 3D, tetrahedrons and hexagonal elements are the most preferred elements. All of these element types were adopted and tried in the developed code. The choice of element type influences the numerical solution strongly. In addition to the element types, the number of nodes on the elements is also crucial in computations. Depending on elemental node numbers, there are two basic element types for quadrilateral and hexagonal elements, being Lagrange type and serendipity type elements [51]. In this work, Lagrange type elements were used. Both in 2D and 3D, linear and quadratic elements were utilized. The node numbers used for linear and quadratic elements are presented in Table 2.1.

Table 2.1 Node Numbers of Different Elements

		Linear	Quadratic
2D	Triangle	3	6
	Quadrilateral	4	9
3D	Tetrahedron	4	10
	Hexagonal	8	27

These 4 element configurations are shown in Figure 2.3 - Figure 2.6.

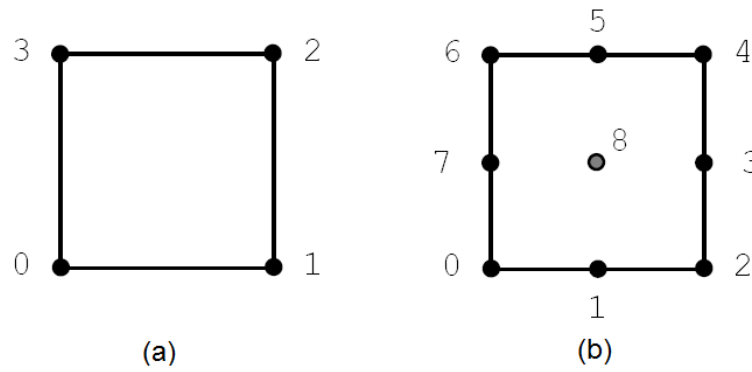


Figure 2.3 Lagrange Type Quadrilateral Elements: (a) Linear, (b) Quadratic [52]

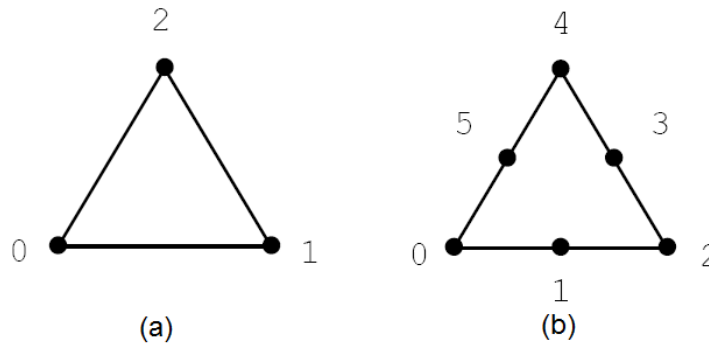


Figure 2.4 Triangular Elements: (a) Linear, (b) Quadratic

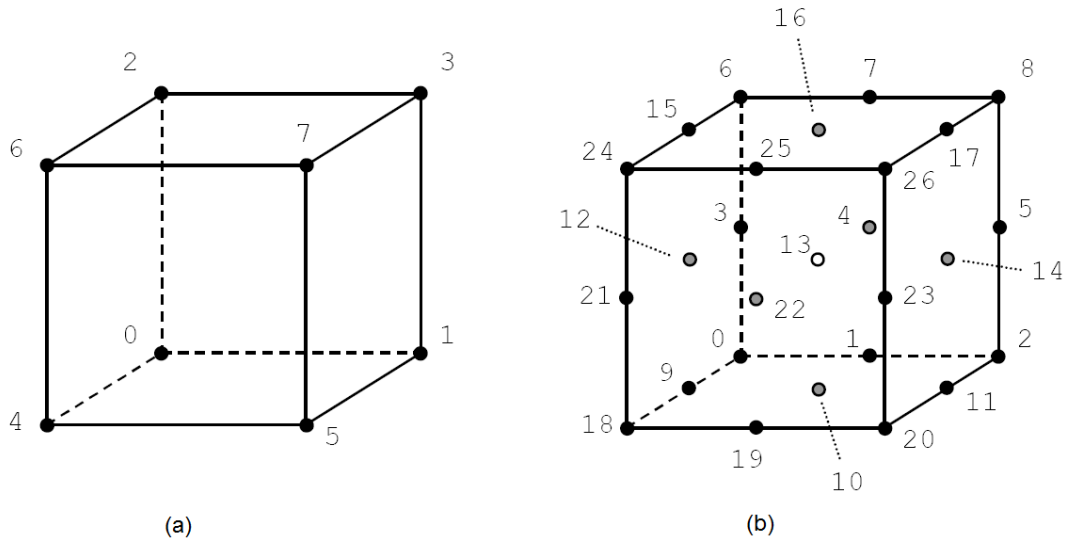


Figure 2.5 Lagrange Type Hexagonal Elements: (a) Linear, (b) Quadratic

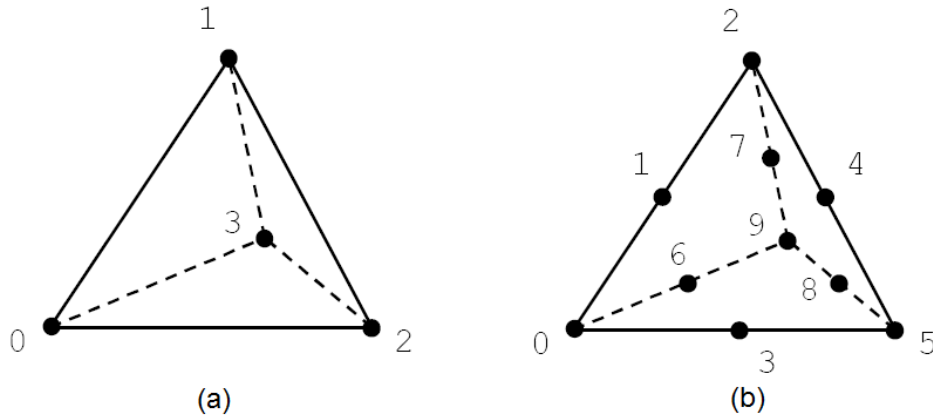


Figure 2.6 Tetrahedron Elements: (a) Linear, (b) Quadratic

In the trial simulations with all these elements, it was seen that only quadrilateral and hexagonal elements gave satisfactory results. Part of this drawback can be explained by the following requirement proposed by Jiang [5]

$$N_{elem} \times N_{Gauss} \times N_{eq} \geq N_{node} \times m - N_{bc} \quad 2.93$$

where N_{elem} is number elements in the domain, N_{Gauss} is the number of Gauss quadrature points used in numerical integrations over elements, N_{eq} is the number of differential equations for the problem, N_{node} is the number of nodes in the domain, m is the number of unknowns at each node and N_{bc} is the number of boundary conditions implemented on the boundaries of the domain. If the number of Gauss

quadrature points chosen is small, this requirement cannot be hold and iterative solver does not converge. Further, if the number of Gauss quadrature points is large and left hand side of the inequality is way higher than the right hand side, then the system becomes overdetermined and leads to underestimated solution. Therefore, the LHS and RHS of the Eqn. (2.93) should be close to each other.

Jiang showed that the above requirement is the reason why linear triangles and tetrahedrons cannot achieve desired results with LSFEM. Even if one-point Gauss quadrature is used, the LHS results in very high numbers compared to RHS and the requirement cannot be satisfied. Hence, Jiang advised the use of high order triangles and tetrahedrons. However, trials in this study showed that it is very difficult to achieve the requirement given in Eqn. (2.93) even with the quadratic triangles and tetrahedrons. Therefore, desired results with triangles and tetrahedrons cannot be obtained.

Simulations with quadratic quadrilaterals and hexagons were proven to be accurate. However, since there are 27 nodes in quadratic hexagonal element, the band width of the resulting global stiffness matrix becomes large. Consequently, the memory requirement of the system increases. In addition, since the number of Gaussian points used in the numerical integration was kept high to satisfy Eqn. (2.93), the time required to obtain stiffness matrix increased dramatically. Therefore, it was decided to use linear quadrilaterals and hexagons in the solution of problems

Since the integral limits of Gauss quadrature integration scheme are -1 to 1, shape functions are also defined in these limits. Elements having these limits are called master elements and transformation from master element coordinates to global coordinates is done using Jacobian of the elements. Linear quadrilateral master element and its coordinates are shown in Figure 2.7.

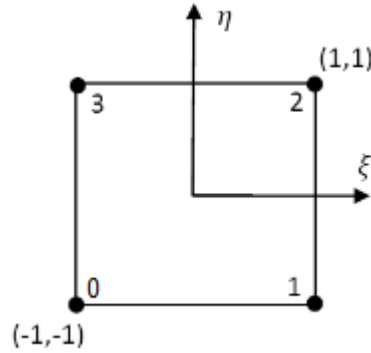


Figure 2.7 Linear Quadrilateral Master Element

Depending on the node number of the element, proper shape functions should be used. The most important feature of the shape functions is their Kronecker-delta property, according to which the shape function associated with a node of the element has the value of 1 on that node and 0 on the other nodes. This can be shown mathematically, for a 1D element, as follows

$$S_i(\xi_j) = \delta_{ij} = \begin{cases} 1 & \text{if } i = j \\ 0 & \text{if } i \neq j \end{cases} \quad 2.94$$

Shape functions for any element can be determined using Kronecker-delta property. For example, for the one dimensional linear element given in Figure 2.8, the shape functions are as follows

$$S_1 = \frac{1}{2}(1 - \xi) \quad S_2 = \frac{1}{2}(1 + \xi) \quad 2.95$$

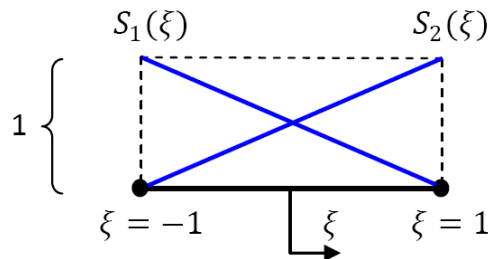


Figure 2.8 1D Master Element and Shape Functions

Shape functions for linear quadrilateral and hexagonal elements can be found by combining the one dimensional shape functions given by Eqn. (2.95).

2.5 Linear Solver and Storage Schemes

As mentioned earlier, LSFEM results in a sparse, symmetric and positive definite (SPD) matrix system, which can be solved by iterative solvers such as the conjugate gradient method efficiently. Efficiency of conjugate gradient method can significantly be improved by the application of preconditioning. The idea behind preconditioning is to improve condition number of the coefficient matrix [53]. For a matrix with SPD property like the stiffness matrix in LSFEM, the preconditioner should be similar to the original matrix and have the same SPD property. The simplest preconditioner is the diagonal of the original matrix and this choice leads to the famous Jacobi preconditioning. There are other preconditioning techniques, like incomplete Cholesky factorization, which improve condition number of the coefficient matrix even more. However, it is time consuming to construct Cholesky factors and then taking the inverse of those factors to be used in preconditioning of conjugate gradient. Therefore, a trade-off analysis between the time spent to apply the incomplete Cholesky and the gain from faster convergence of conjugate gradient should be made. For the sake of simplicity, Jacobi preconditioned conjugate gradient solver was used in this study. Implementation of incomplete Cholesky conjugate gradient might be a future improvement.

Since the number of elements required to solve fluid flow and heat transfer problems in three dimensions is high, the coefficient matrix can occupy terabytes of memory if it is stored in full version. To solve this problem, two methods were applied. The first one is to store only the elemental stiffness matrices instead of one large global matrix and apply the conjugate gradient solution in an element by element (EBE) manner; and the second solution is to store the global stiffness matrix using a sparse storage scheme.

In EBE solution, the elemental stiffness matrices were formed and stored. The time consuming matrix vector multiplication of the conjugate gradient solution was performed using the elemental stiffness matrices, without forming the global stiffness matrix at all. If the system to be solved is extremely large that even the storage of elemental matrices exceeds memory limits, elemental stiffness matrices can be formed during conjugate gradient iterations and can be removed from the memory

after being used. However, this way the computation time increases drastically. As an alternative to EBE solution, it is possible to store the global stiffness matrix in the memory using a sparse storage scheme and perform matrix vector product operation of the conjugate gradient solver at the global level. Among many sparse storage schemes, compressed row storage scheme was used in this study [54].

In both EBE and sparse storage solutions, only the lower halves of the elemental and global stiffness matrices were stored, benefiting their symmetric structure. In order to decrease the time requirements while solving the equations, it was decided to use a third party library to perform basic linear algebra operations. For this purpose, Basic Linear Algebra Subprogram (BLAS) routines of Intel[®] MKL were used [55]. These routines are best suited for matrix-vector products in the developed code when sparse storage scheme is used. Considerable time reduction in computations was achieved when Intel[®] MKL was utilized.

Trying to achieve both low computation times and memory requirements; sparse storage scheme based on compressed row storage and Jacobi preconditioned conjugate gradient solver supplemented with Intel[®] MKL were used in most of the simulations mentioned in the next chapters.

In order to provide an insight about the memory requirements and the speed of the developed codes, RAM consumption and time elapsed in the solution of microchannel heat transfer problem were recorded. Simulations were conducted using a computer with Intel Xeon E5-2670 CPU's. The speed of each CPU is 2.6 GHz and 8 cores were utilized in the calculations. For the solution of a domain composed of 119040 elements, 193 MB of memory was used. The flow solution takes 22 minutes whereas the heat transfer solution takes 166 minutes. The speed of heat transfer solver was low because very high number of conjugate gradient iterations was required to obtain convergent results.

CHAPTER 3

CODE VALIDATION

To check whether the codes can successfully solve viscous incompressible flow and heat transfer problems, some benchmark problems found in the literature were solved and the results are presented in this chapter.

3.1 Flow Solver Validation

Two very famous benchmark problems for incompressible flows were solved and the obtained results were compared with the available data in the literature. These problems are lid driven cavity flow and backward facing step flow.

3.1.1 3D Lid Driven Cavity Flow

The problem simulates the flow inside a cubical cavity with all the faces being stationary except the top one, as shown in Figure 3.1. The top wall was given a velocity of 1 m/s in the x -direction. Zero reference pressure was specified on the middle of the bottom wall. All the edges of the cubical cavity were taken as 1 meter in length. The computations were performed for Reynolds numbers of 100 and 1000. An imaginary fluid with a density of 1 kg/m^3 was used and the desired Reynolds numbers were obtained by varying the viscosity.

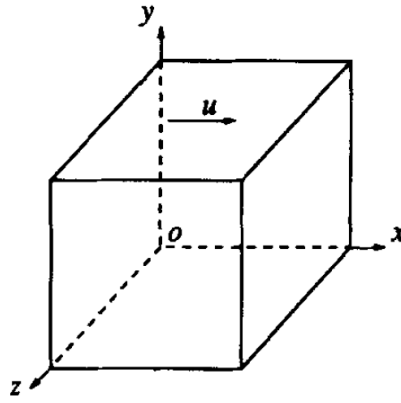


Figure 3.1 Configuration for 3D Lid Driven Cavity Flow [7]

A non-uniform mesh with 125000 ($50 \times 50 \times 50$) elements was used. The elements get finer as they get close to the wall regions. Mesh for the top wall is presented in Figure 3.2. All other walls had the same mesh and a structured mesh of hexagonal elements was obtained for the entire volume based on these face meshes.

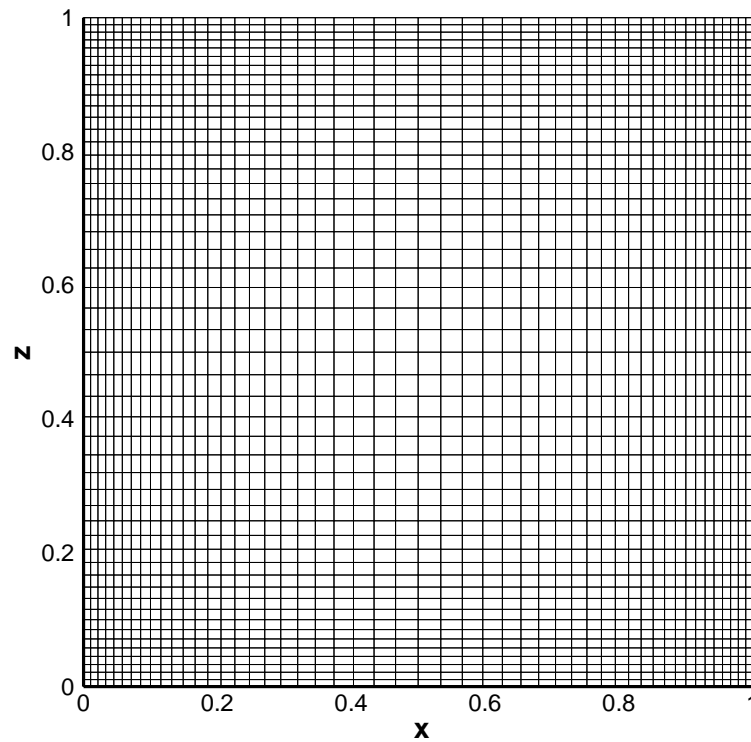


Figure 3.2 Non-Uniform Top Wall Mesh for 3D Lid Driven Cavity Flow

As convergence criterion, tolerances of 10^{-5} and 10^{-8} were selected for Newton iterations and conjugate gradient solver respectively. Converged solutions were obtained for both Reynolds numbers.

The u - and v -velocity contours at $z = 0.5$ plane for Reynolds number 100 are given in Figure 3.3.

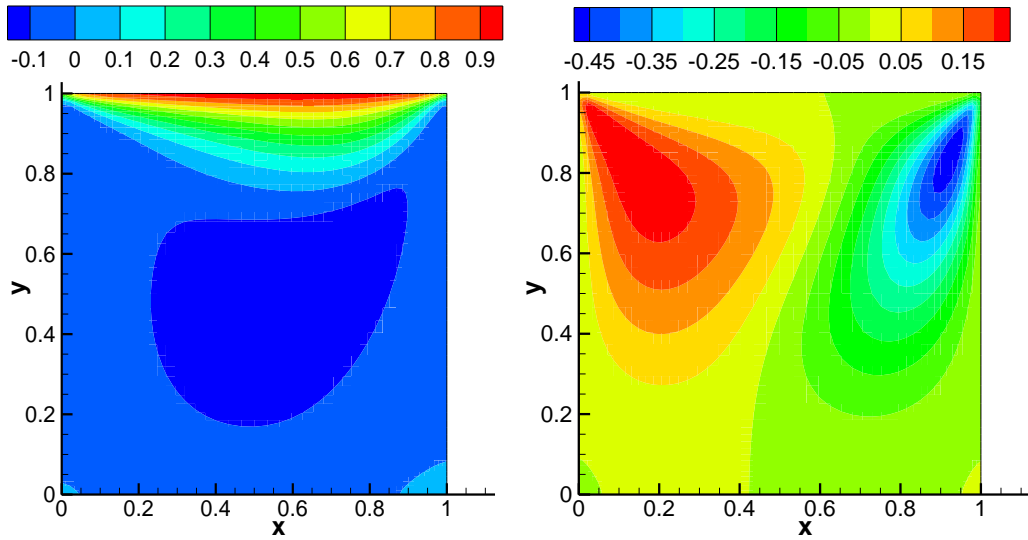


Figure 3.3 u - and v -velocity Contours at $z = 0.5$ for $Re = 100$

In several works in the literature [5, 7, 56-58], u -velocity profiles on $x = z = 0.5$ line and v -velocity profiles on $y = z = 0.5$ line were presented. To check the accuracy of results obtained with the code, comparison with data from Jiang [5] and Yang et al. [56] were made. Jiang used LSFEM as in this work, whereas Yang et al. used implicit weighted ENO scheme to solve the Cavity problem. In Figure 3.4, u and v -velocity profiles for Reynolds number of 100 are presented on $x = z = 0.5$ and $y = z = 0.5$ lines, respectively. Since Jiang did not provide v -velocity values, only results from Yang et al. are presented. A similar comparison for $Re=1000$ is presented in Figure 3.5.

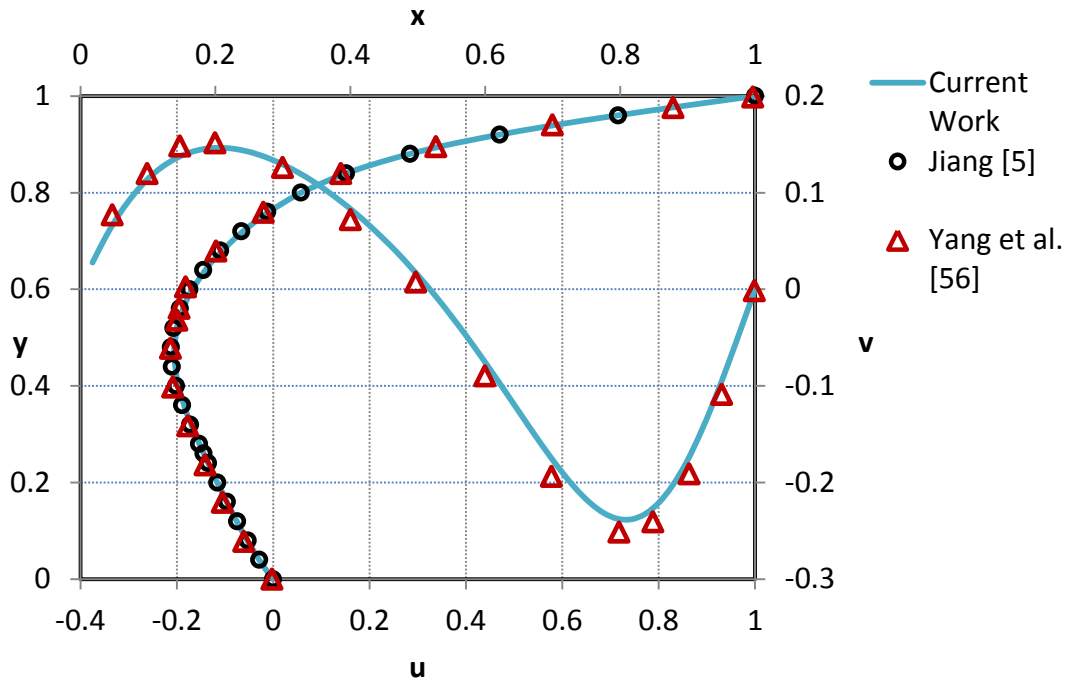


Figure 3.4 Velocity Profiles along Centerlines for $Re=100$

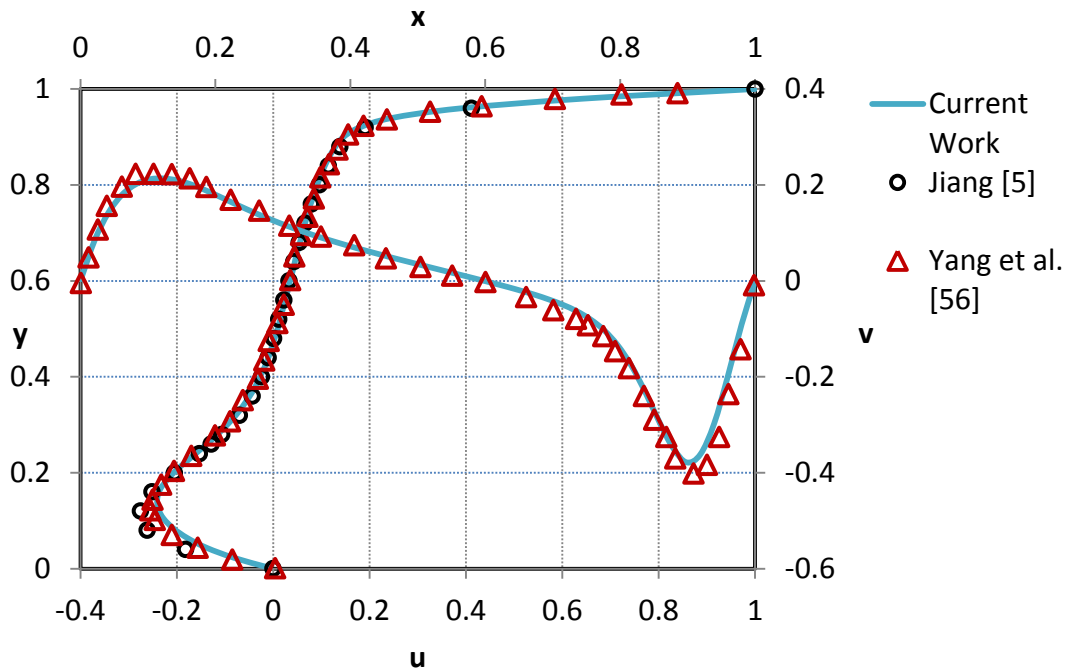


Figure 3.5 Velocity Profiles along Centerlines for $Re=1000$

Although results are in good agreement in general, there are slight differences especially in predicting maximum velocities along centerlines. This might be due to

differences in the grids used. Jiang discretized the computational domain into a $50 \times 50 \times 50$ uniform mesh. He added 2 layers of mesh near top wall in order to achieve more resolution and obtained a mesh of $50 \times 52 \times 50$ nodes. On the other hand, Yang et al. used $33 \times 33 \times 33$ non-uniform mesh which gets denser near all walls as in this work.

3.1.2 Backward Facing Step (BFS) Flow

Although the solver was proven to be successful in the simulation of 3D lid driven cavity flow, it was still necessary to test it with an inlet-outlet type benchmark problem. This is because LSFEM has problems in mass conservation as stated earlier and one cannot test it with flow simulation inside the cavity. Furthermore, since one of the main motivations in this work is to be able to develop a code to simulate microchannel heat transfer problems, it is obligatory to test the flow solver with an inlet-outlet type problem. Therefore, it was decided to solve another well-known benchmark problem for incompressible flow solvers, namely the backward facing step (BFS) flow.

In BFS problem, the fluid coming from a narrow channel flows into a wider one and experiences a sudden expansion as seen in Figure 3.6. Due to this sudden expansion, there occurs circulation regions and prediction of detachment and reattachment points becomes important. There are many versions of BFS flow with different expansion ratios (h/H). In the experimental work of Armaly et al. [59], an expansion ratio of 1/1.94 was used and that is the one simulated in this work.

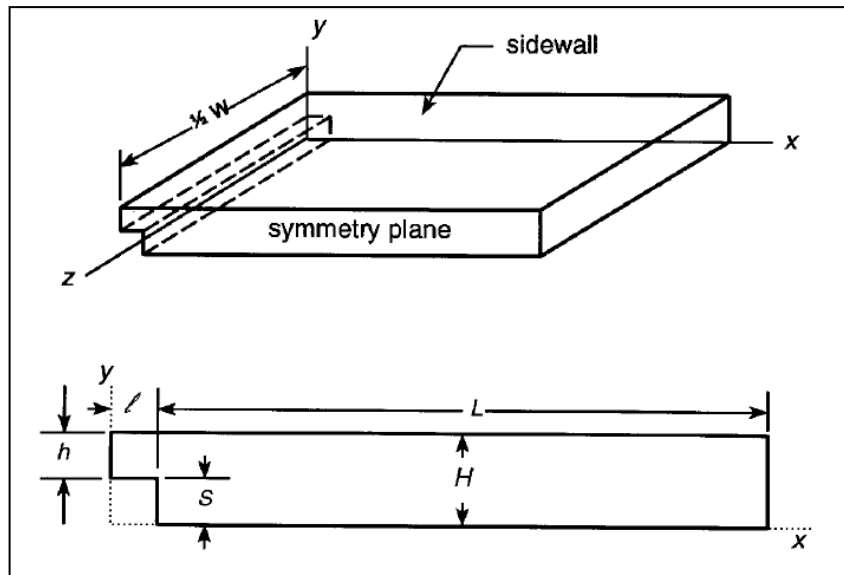


Figure 3.6 Geometric Parameters of the Backward Facing Step Flow [60]

The values of geometric parameters shown in Figure 3.6 are given in Table 3.1.

Table 3.1 Values of Geometric Parameters for BFS Problem

L	l	H	h	S	W
200 mm	100 mm	10.1 mm	5.2 mm	4.9 mm	180 mm

A large number of researchers solved BFS problem in 2D and 3D (see Table 1 of [60]). Since most of the researchers referenced Armaly et al.'s experimental work [59], and the most comprehensive numerical work simulating the same geometry is Williams and Baker's study [60], most of the results of the current study were compared with these two references. Reattachment length results were also compared with Jiang et al.'s [61] and Ku et al.'s [62] works. Again Jiang et al. used LSFEM as in this work, whereas Williams and Baker implemented continuity constrained method and Ku et al. used pseudo-spectral matrix element method.

The problem was solved for different Reynolds numbers up to 700. While calculating Reynolds number, mean velocity at the inlet was taken as reference velocity and twice the height of entrance region was used as hydraulic diameter. The primary reattachment length shown in Figure 3.7 and velocity at different x stations were computed and compared with the available data from references. Since the flow is

symmetric up to the Reynolds number of interest, the half domain in z -direction was solved and symmetrical boundary condition was applied. The symmetry plane can be seen in Figure 3.6. At the exit of the domain, fully developed boundary conditions were applied and reference pressure was specified as zero. The working fluid is air and its properties together with hydraulic diameter are given in Table 3.2.

Table 3.2 Flow and Fluid Properties for BFS Flow

ρ	μ	D_h
1.205 kg/m^3	$1.785 \times 10^{-5} \text{ Pa}\cdot\text{s}$	10.4 mm

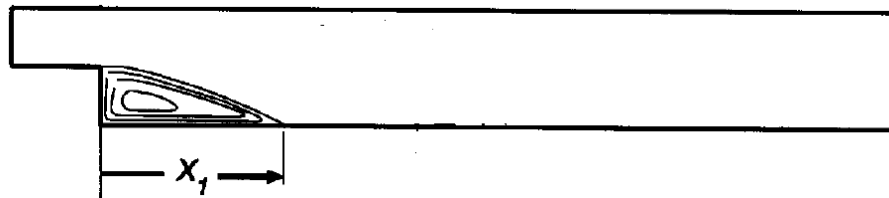


Figure 3.7 Primary Circulation Region and Reattachment Length [60]

The computational domain was composed of $50 \times 11 \times 30$ structured mesh for entrance region and $80 \times 21 \times 30$ structured mesh for the region after the step, a total of 66900 elements. Elements were clustered near step, entrance and wall regions. Surface meshes for $x - y$, $x - z$ and $y - z$ planes are given in Figure 3.8 (ratios of coordinate axes are not to scale).

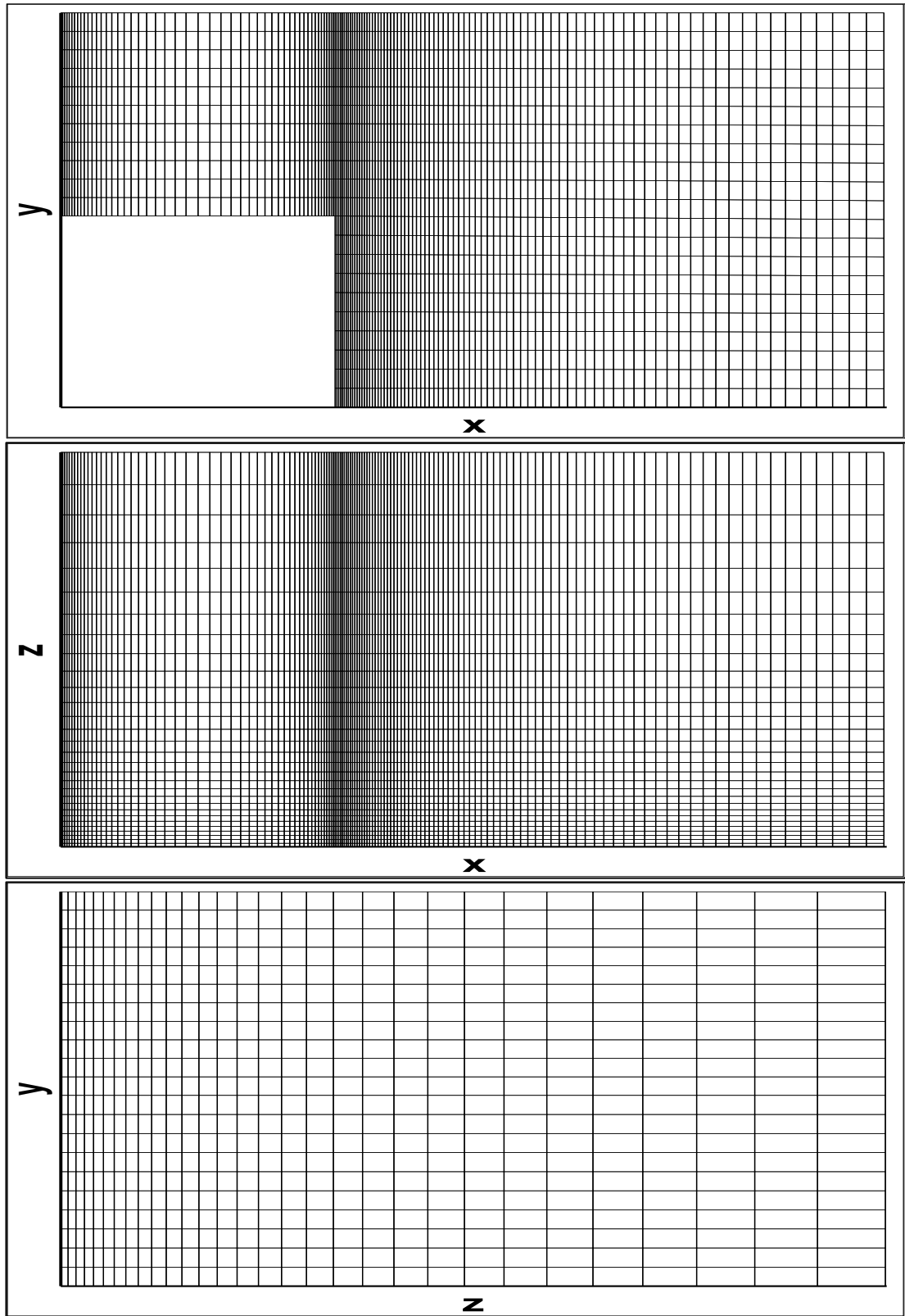


Figure 3.8 Surface Mesh for $x - y$, $x - z$ and $y - z$ Planes of BFS Problem

In their work, Williams and Baker used $4 \times 11 \times 24$ and $87 \times 20 \times 24$ mesh for upstream and downstream of the step, respectively. The reason of large difference between the numbers of streamwise edge meshes upstream of the step between present work and Williams and Baker's is that, a uniform velocity was given at the inlet in this work whereas Williams and Baker used fully developed inlet velocity profile. Uniform inlet was preferred in the current study because it is uncertain whether Williams and Baker's inlet profile was parabolic in both y and z directions, or only in y direction.

To calculate the reattachment length after the step, a point where the u -velocity is zero was sought. The length between the step and the zero u -velocity point was set as reattachment length. In order to observe how the developed code predicts primary reattachment length, results from other works were compared with the current one and the results are presented in Figure 3.9. Note that the reattachment length, x_1 , was normalized with the step height, S .

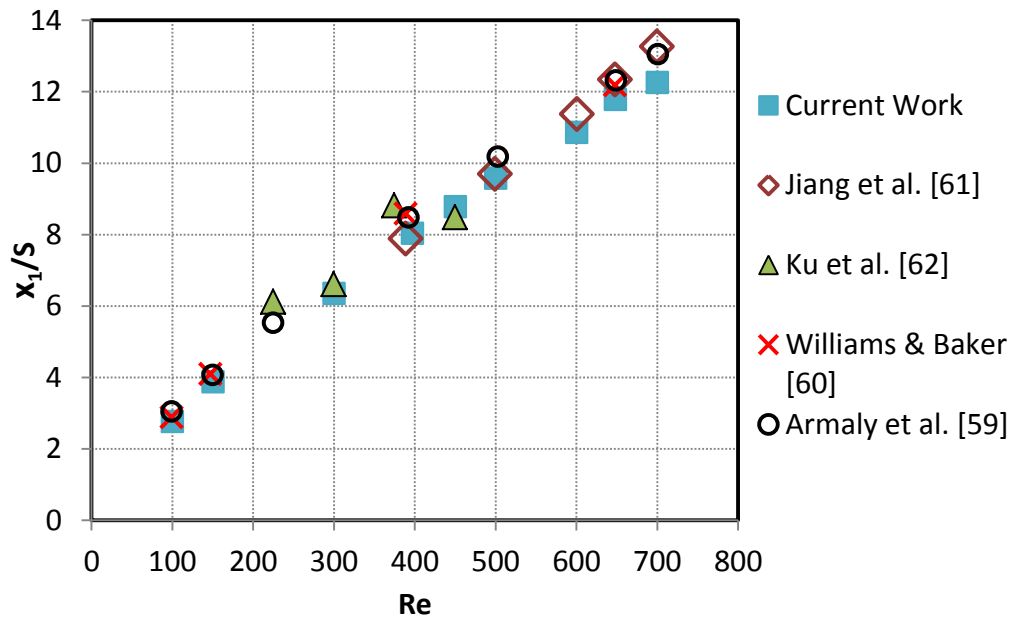


Figure 3.9 Change of Primary Reattachment Length with Reynolds Number

As can be seen from Figure 3.9, developed code predicted the change of primary reattachment length with Reynolds number successfully. There is a slight difference only at Reynolds number of 700. Although a denser mesh around the possible

reattachment point was used, no further improvement was observed in predicting reattachment length.

For Reynolds number of 648, change of primary reattachment length in z direction is presented in Figure 3.10. Note that z coordinate was normalized by half width, $W/2$. The agreement between the results of Armaly et al. and the present work can be seen in the figure. The change of reattachment length in z -direction shows the three dimensionality of flow in this Reynolds number regime. As can be seen, there is a difference at Armaly et al.'s results in reattachment length between Figure 3.9 and Figure 3.10. This might be due to a mistake Armaly et al. made while presenting their results.

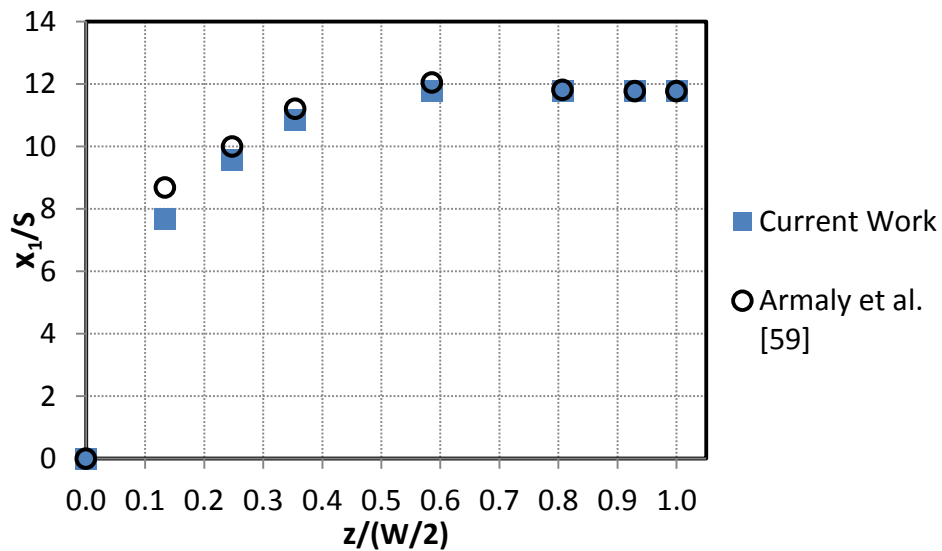


Figure 3.10 Change of Primary Reattachment Length in z -direction at $Re=648$

In addition to reattachment length results, the changes of u -velocities in z -direction at different x and y stations were also compared. These comparisons further show how accurately the code predicts flow structure in the domain. All the presented results are for Reynolds number of 648. First of all, in Figure 3.12, u -velocity profile along z -direction at just above the step, i.e., $x_1/S = 0$, is given for 3 different y values. It is seen that the u -velocities computed by the code are consistent with the experimental data except at $y = 8.55$ mm. Although different mesh resolutions were tried to solve this problem, the results could not be further enhanced and the reason

for this incompatibility could not be found. Figure 3.11 shows the points where the compared velocities were extracted in z-direction.

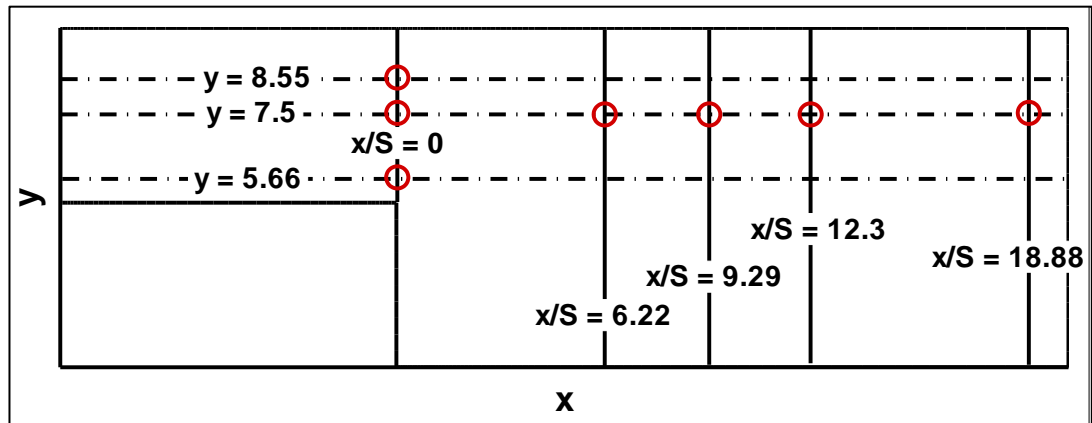


Figure 3.11 The Points through Which u -Velocities are Compared in z -Direction

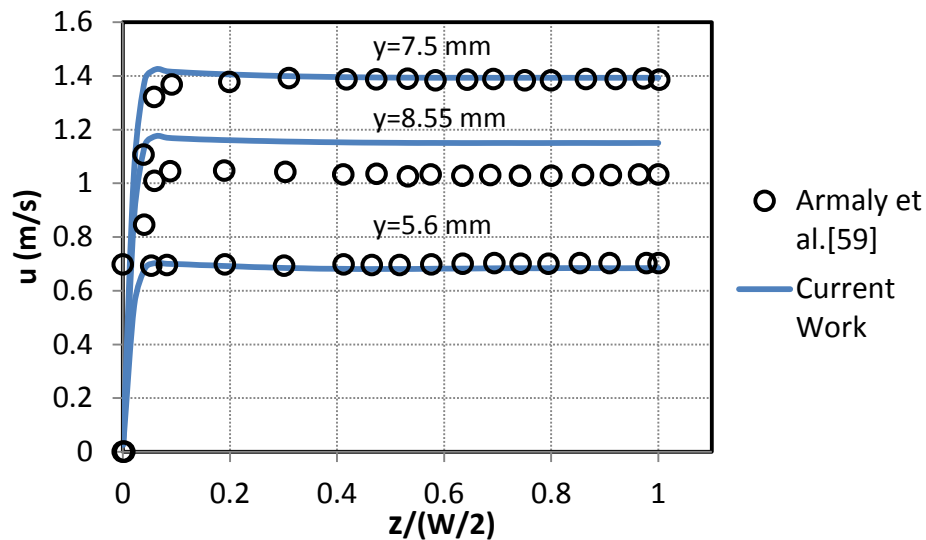


Figure 3.12 Change of u -Velocities along z -Direction at $x_1/S = 0$ and Different y -Stations, $Re=648$

In Figure 3.13, changes of u -velocities along z -direction at $y = 7.5$ mm and different x -stations are given. This time however, the results of Williams and Baker's work [60] are also present. Again the velocities are for Reynolds number of 648. The results obtained with the developed code are well consistent with experimental and numerical data. In addition, it is clear that flow field is strongly three dimensional for this Reynolds number regime as Armaly et al. [59] claimed. Due to the fact that Armaly et al. probed velocity values near wall with very few points, they missed the

flow reversals which were caught by both the current code and Williams and Baker's.

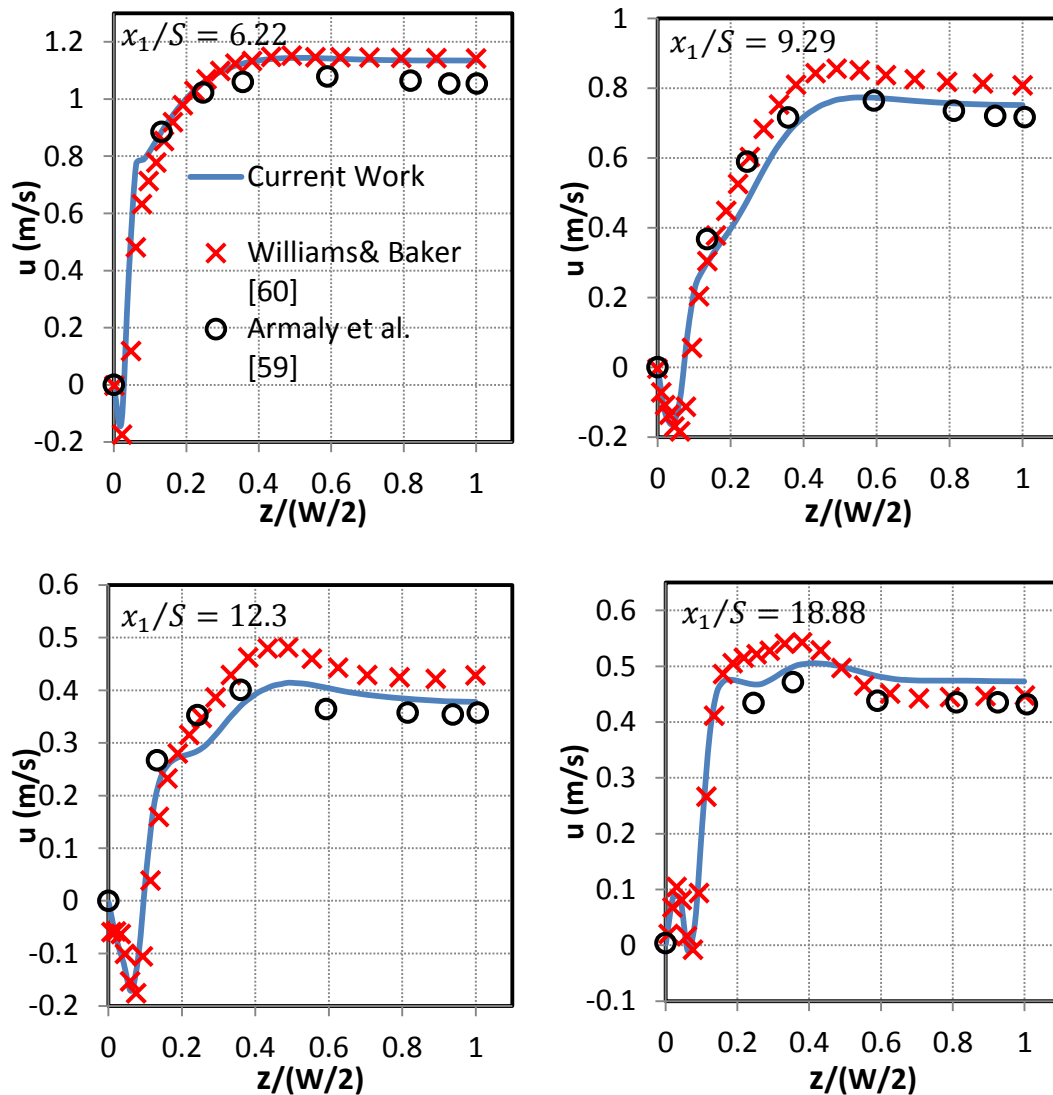


Figure 3.13 Change of u -Velocities along z -Direction at $y = 7.5$ mm and at different x -Stations, $Re=648$

By solving backward facing step problem in 3D successfully, the code proved to be sufficient for the solution of inlet-outlet type flow problems. It should be noted that the velocity values at both inlet and outlet of the channel were checked and there occurred no deterioration in mass conservation. Therefore, no additional treatment was done to ensure continuity for this problem.

3.2 Heat Transfer Solver Validation

For incompressible flows, benchmark heat transfer problems found in the literature are mostly coupled with fluid flow through natural convection. No fully trustable benchmark problem solving fluid flow and heat transfer in an uncoupled manner could be found. Therefore, it was decided to develop a coupled code and test it by solving the 3D thermally driven cavity flow.

3.2.1 Thermally Driven Cavity (TDC) Flow

In this benchmark problem, the natural convection inside a differentially heated cubical cavity is analyzed. One of 6 surfaces of the cube is heated whereas the opposite wall is cooled. All other 4 surfaces are kept adiabatic. The general view of computational geometry and boundary conditions is given in Figure 3.14.

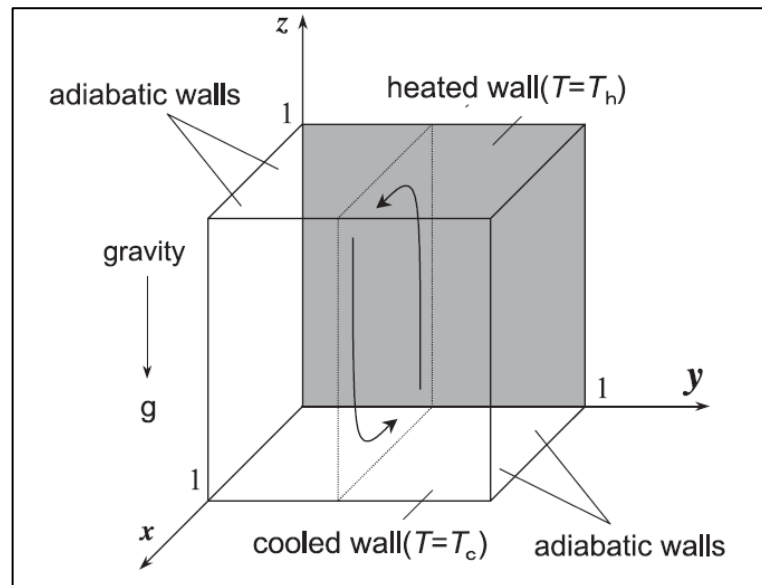


Figure 3.14 General Geometry and Boundary Conditions for TDC Flow [63]

Due to the heated wall, the fluid nearby gets hotter and lighter, and therefore moves in opposite direction of gravity. The heated fluid faces the cooled wall on the opposite side and gets colder and denser, and moves down in the direction of gravity. This way the heat inside the cavity is convected and different flow and temperature profiles occur depending on Rayleigh and Prandtl number of the fluid. Consequently, accurate prediction of temperature and velocity changes inside the cavity is an important evaluation criterion for the developed code.

For the TDC problem, air was selected to be the working fluid. Prandtl number was set to be 0.71, Froude number became 1 and the problem was solved for Rayleigh numbers of 10^4 , 10^5 and 10^6 . Computational grid was the same as in the lid driven cavity problem, i.e., a grid of 125000 structured elements clustered near the wall regions (see Figure 2.1).

In Figure 3.15 and Figure 3.16, u and w velocities along centerlines in z and x directions respectively are presented. The Rayleigh number of interest in figures is 10^5 .

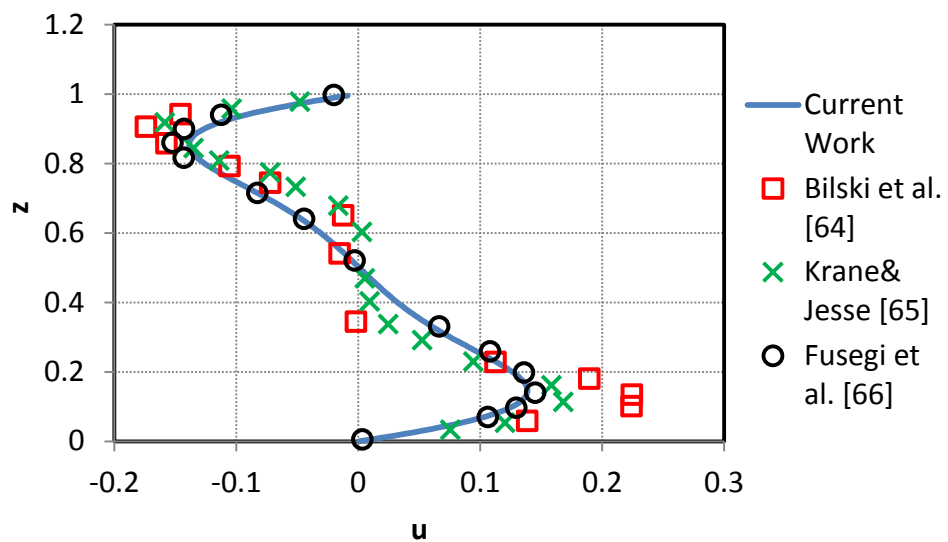


Figure 3.15 Comparison of u -Velocities along Centerline in z -Direction, $Ra=10^5$

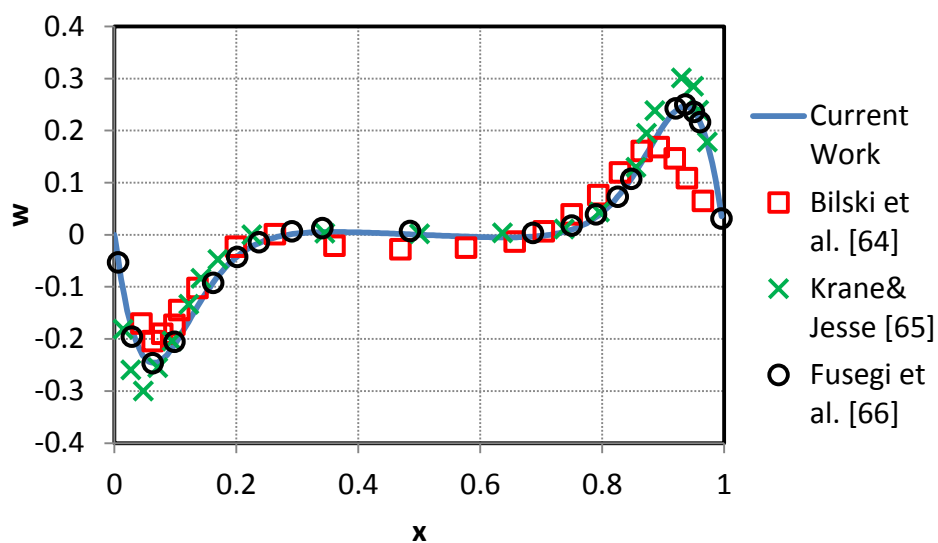


Figure 3.16 Comparison of w -Velocities along Centerline in x -Direction, $Ra=10^5$

The work of Bilski et al. [64] and Krane and Jesse [65] were of experimental type and were conducted at Rayleigh numbers of 1.03×10^5 and 1.89×10^5 respectively. Fusegi et al. [66] solved the problem using a finite difference scheme and investigated the effect of boundary condition types given for horizontal walls. They employed a computational grid of $62 \times 62 \times 62$. Fusegi et al. claimed that the horizontal walls in experimental setups cannot be insulated perfectly and this might be the source of difference in this velocity comparison. Indeed, they used a conducting wall boundary condition for the top and bottom wall and the results of that case were closer to experimental findings. Therefore, it is better to compare the results of the current work with that of Fusegi et al. In that perspective, the results obtained here are highly satisfactory.

In Figure 3.17, the temperature contours for $Ra=10^6$ are compared with the work of Wakashima and Saitoh [63]. In their study, Wakashima and Saitoh implemented a so called time-space method and used a computational grid of $120 \times 120 \times 120$. Temperature contours at $y = 0.5$ reveal that there is a high consistency between the current work and the reference study.

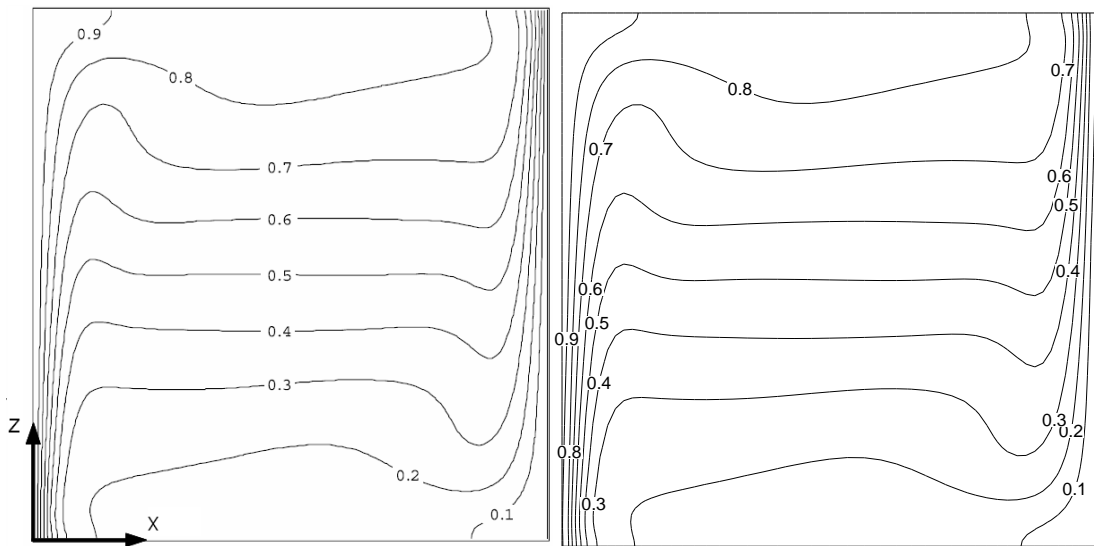


Figure 3.17 Temperature Contours for $Ra=10^6$ at $y = 0.5$, Wakashima and Saitoh [63] (left), Current Work (right)

For a final comparison of TDC results, maximum velocities along centerlines and their positions together with y -vorticities at the center of the cavity are given in

Table 3.3 for all Rayleigh numbers. Although there are slight differences in some values, these differences do not exceed 5% and therefore the results are consistent with other works.

Table 3.3 y -Vorticity at the Center of the Cavity, Maximum Velocities and Their Positions along Centerlines

	Study	ω_y	u_{max} (z location)	w_{max} (x location)
$Ra = 10^4$	Wakashima and Saitoh [63]	1.1018	0.1984 (0.8250)	0.2216 (0.1167)
	Fusegi et al. [66]	-	0.2013 (0.8167)	0.2252 (0.1167)
	Current Work	1.0645	0.1933 (0.8286)	0.2179 (0.1150)
$Ra = 10^5$	Wakashima and Saitoh [63]	0.2576	0.1416 (0.8500)	0.2461 (0.0667)
	Fusegi et al. [66]	-	0.1468 (0.8547)	0.2471 (0.0647)
	Current Work	0.2442	0.1387 (0.8538)	0.2456 (0.05973)
$Ra = 10^6$	Wakashima and Saitoh [63]	0.1366	0.0811 (0.8583)	0.2587 (0.0333)
	Fusegi et al. [66]	-	0.08416 (0.8557)	0.2588 (0.0331)
	Current Work	0.1338	0.08169 (0.8538)	0.2583 (0.0346)

The overall performance of natural convection solver is pretty well and the heat transfer solver can be regarded as validated.

3.3 Conjugate Heat Transfer Solver Validation

Again, there could not be found a widely solved conjugate heat transfer benchmark problem to be simulated in the literature. Instead, the conjugate heat transfer modeling capability of the developed code was tested with two simple two dimensional problems. The first one is again a natural convection inside the cavity problem with a solid region adjacent to the cavity. Second problem is the well-known Couette problem with a heated solid part at the bottom. Details of the problems and the results in a comparative way are presented in the next two subsections.

3.3.1 Conjugate Heat Transfer in Thermally Driven Cavity Flow

The problem domain is given in Figure 3.18.

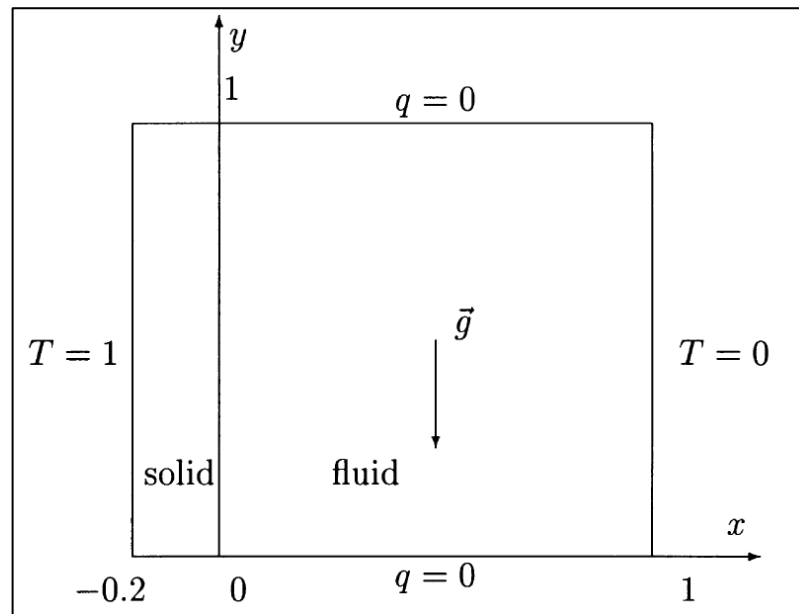


Figure 3.18 General View of Thermally Driven Cavity with Conjugate Heat Transfer [38]

As can be seen from Figure 3.18, in addition to the standard cavity, there is a solid region on the left and the left side of the solid is heated whereas the right of the fluid domain is cooled. Other surfaces are kept insulated and no-slip boundary condition is given for all the walls. Velocity values in the solid region are set to zero.

For the fluid regions, the equations to be solved are 2D versions of Eqn. (2.15-2.17). For the solid region on the other hand, only the Eqn. (2.17) was solved with a slight

modification. The term $1/Pe$ was multiplied with the ratio of thermal conductivity of solid to that of fluid. The convective part in Eqn. (2.17) vanished in the solid part since the velocities were set to zero before the calculations.

The mesh used for the fluid region was the same as given in Figure 3.2. For the solid part, 10×50 elements clustered near the interface and boundaries were used.

Working fluid was air and the Prandtl number was 0.71. Calculations were performed for Rayleigh number of 71000. Three different thermal conductivity ratios, i.e., K were examined. The temperature contour for $K = 1$ was compared with the work of Hribersek and Kuhn [38] and is presented in Figure 3.19.

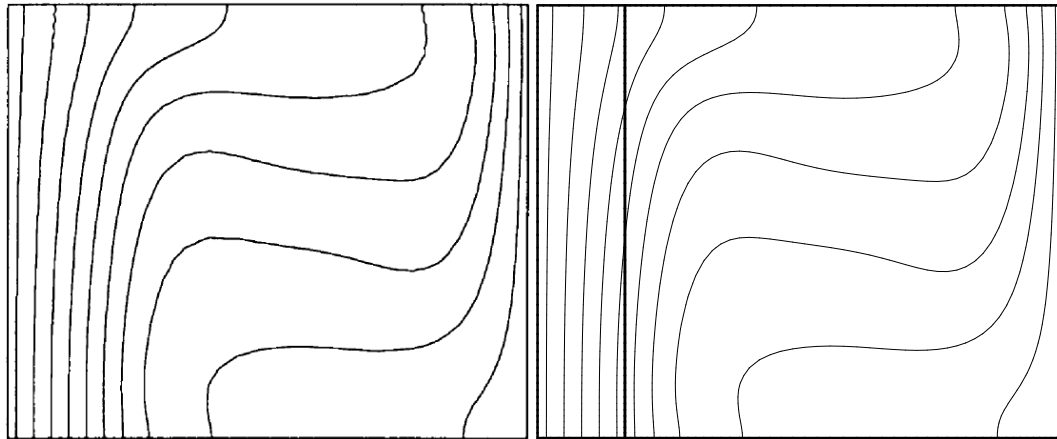


Figure 3.19 Comparison of Temperature Contours for $K = 1$ and $Ra = 71000$ Hribersek & Kuhn [38] (left), Current Work (right)

The high consistency between the two solutions can be seen from Figure 3.19. The temperature values along the solid-fluid interface was also recorded and is given in Figure 3.20.

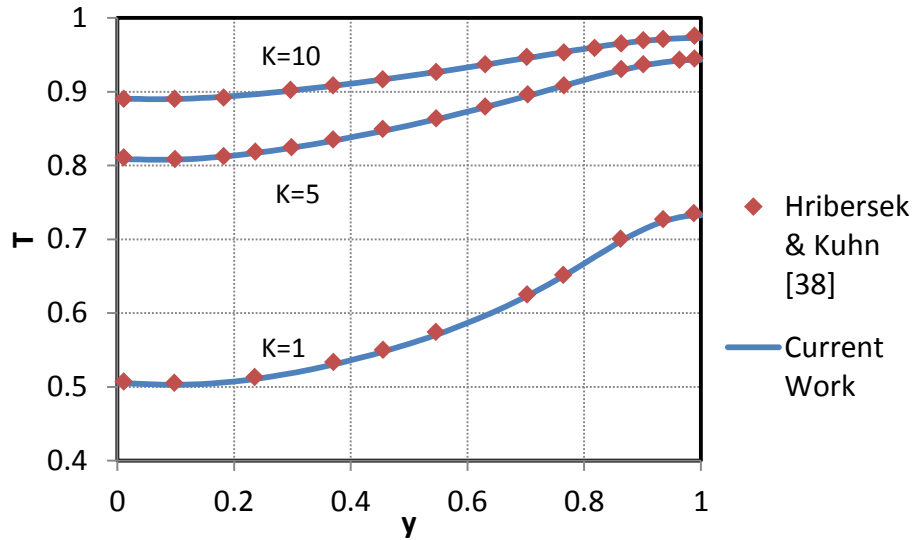


Figure 3.20 Temperature Distribution along the Interface for Different K

The temperature distributions along the interface also reveal that the developed code predicted the temperature profiles for conjugate problems successfully as well.

3.3.2 Conjugate Heat Transfer in Couette Flow

The last problem to be solved before the simulation of a microchannel was the Couette flow with conjugate heat transfer. In this problem, a heated solid region was added to the bottom of the well-known Couette flow and temperature profiles for different thermal conductivity ratios were examined. Problem domain is shown in Figure 3.21.

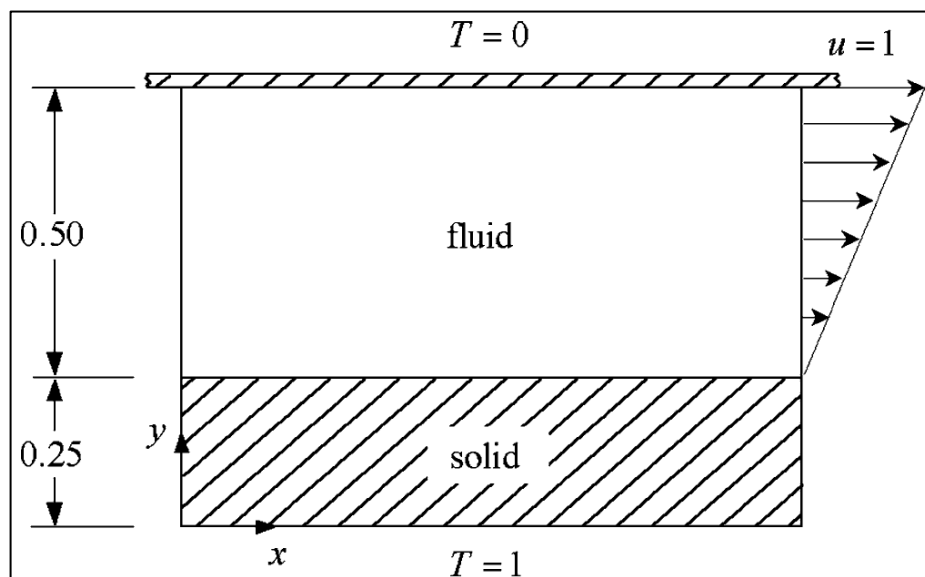


Figure 3.21 General View of Couette Flow with Conjugate Heat Transfer [36]

As seen from the figure, the top plate was moved in positive x -direction with a velocity of 1 m/s. The fluid flow was periodic, i.e., the inlet flow profile was the same as the exit flow profile. Velocities were zero at the fluid-solid interface. Bottom of the solid was kept at non-dimensional temperature of 1 whereas the top of the fluid was at 0 temperature. A 40×30 uniform mesh was used for the whole domain.

Only the fluid domain was solved initially and resultant velocity values were exported to the heat transfer solver. Since no details were presented in Wansophark et al.'s work [36], all fluid properties of interest were taken as 1. The temperature profile in y -direction was extracted and compared with the analytical results of reference [40]. The results for different thermal conductivity ratios are given in Figure 3.22.

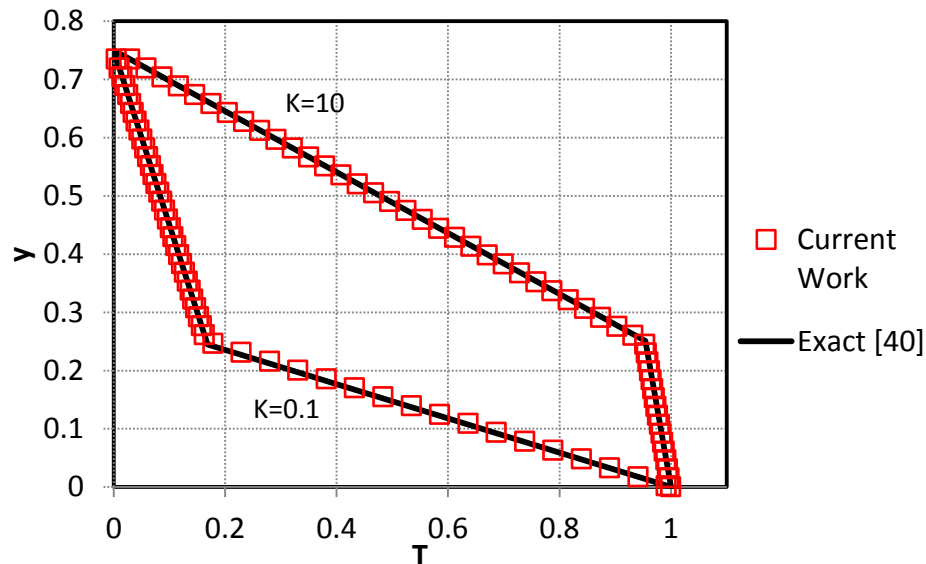


Figure 3.22 Temperature Profiles for Couette Flow in y -Direction for Different K

Again there is an excellent agreement between the current findings and the exact results from White [40]. After all these validations, the code developed proved to be suitable for simulation of inlet-outlet type fluid flow and conjugate heat transfer phenomena. Therefore, it was time to model a real life microchannel heat transfer problem.

CHAPTER 4

SIMULATION OF CONJUGATE HEAT TRANSFER IN A MICROCHANNEL

Since the developed flow and conjugate heat transfer solvers were validated through a comprehensive work, a microchannel heat transfer problem could be modeled. As part of it is explained in the introduction, a number of studies involving numerical and/or experimental conjugate microchannel heat transfer are present [42, 45-48, 67]. Among these works, Kawano et al.'s [46] and, Fedorov and Viskanta's [42] were examined in detail. It was because both studies investigated the same microchannel configuration and, the computational and experimental methods were explained clearly.

In the experiments, Kawano et al. first formed a microchannel and tested it, and then they used it in a real application for cooling electronic equipment. The general view of the tested microchannel is shown in Figure 4.1.

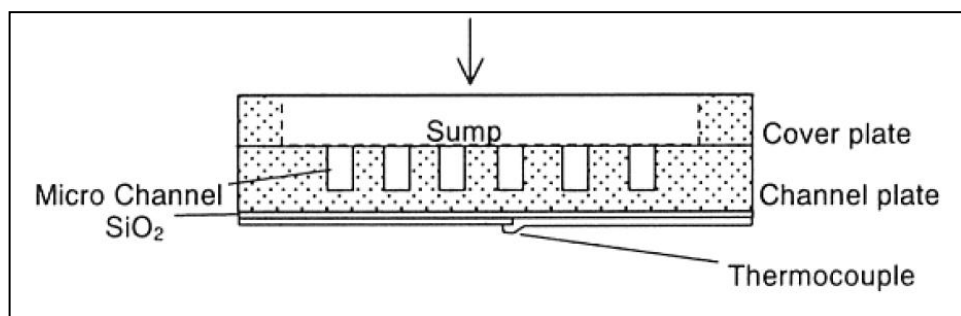


Figure 4.1 Tested Microchannel by Kawano et al. [46]

There were 110 channels in the system in total. The microchannel was made up of Silicon, whereas a Silicon dioxide (SiO_2) film was placed between the channel and thermocouples for electrical isolation.

Two important factors that characterize the performance of a microchannel are Poiseuille's constant (C) and thermal resistance (R_t). Poiseuille's constant is directly related to pressure loss and therefore critical in determining pump power whereas the thermal resistance is crucial in evaluating cooling capabilities of the microchannel. Poiseuille's constant is defined as

$$C = fRe = \frac{2\Delta p D_h}{\rho L u_m^2} \quad 4.1$$

where Δp is the pressure drop through the channel, D_h is the hydraulic diameter of the channel, L is the channel length and u_m is the mean velocity at the inlet. In the experiments, Poiseuille's constant was measured without heat flux input. Therefore, to make proper comparisons, Poiseuille's constant was calculated for no heat input case in Fedorov and Viskanta's computations as well.

Fedorov and Viskanta studied only a single channel of this heat exchanger as seen in Figure 4.2 [42], which was also the problem geometry simulated in the current work. The dimensions of the geometric parameters shown in this Figure 4.2 are given in Table 4.1.

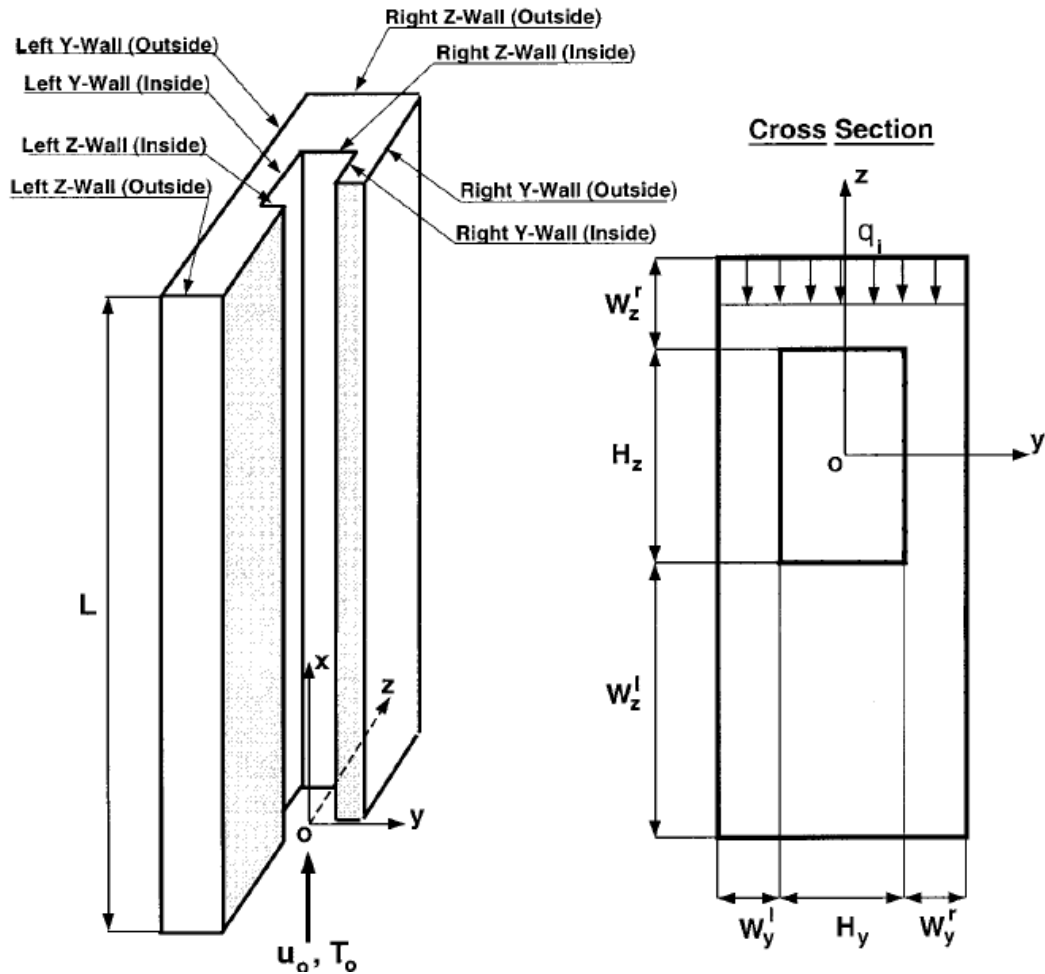


Figure 4.2 Geometry and Boundaries for Single Microchannel to be Simulated [42]

Table 4.1 Geometrical Dimensions of Single Channel

H_z	H_y	W_z^r	W_z^l	W_y^r	W_y^l	L
180 μm	57 μm	270 μm	450 μm	21.5 μm	21.5 μm	10 mm

Fedorov and Viskanta performed a mesh independency study and used a final mesh of $100 \times 16 \times 32$ nodes in x , y and z directions for the whole domain including fluid and solid regions. In the present study, a mesh with the same number of elements with Fedorov and Viskanta's work was tried initially. However, since the grid had only 6 elements on the left z -wall in z -direction, there occurred a large size difference between the adjacent fluid and solid meshes. As the heat transfer in fluid and solid regions were solved in a fully coupled manner in this study, the number of elements in the z -direction in solid was increased to make adjacent fluid and solid

cells of comparable sizes. In addition, to prevent very high aspect ratio meshes at the end of domain in x -direction where exit thermal boundary condition was applied, the number of element in x -direction was increased and the nodes were clustered a bit through the exit of the domain. Making the above mentioned adjustments, a final mesh of $120 \times 16 \times 62$ elements was used. The meshes at x , y and z planes are shown in Figure 4.3. Note that the axis ratios are not to scale. Due to this fact, very high aspect ratios of the elements cannot be observed from Figure 4.3. The highest aspect ratio occurring in the domain is almost 50, which is very large. As can be seen from Figure 4.3, the elements are much denser at the entrance region. This structure was formed on purpose to resolve thermal and flow development properly.

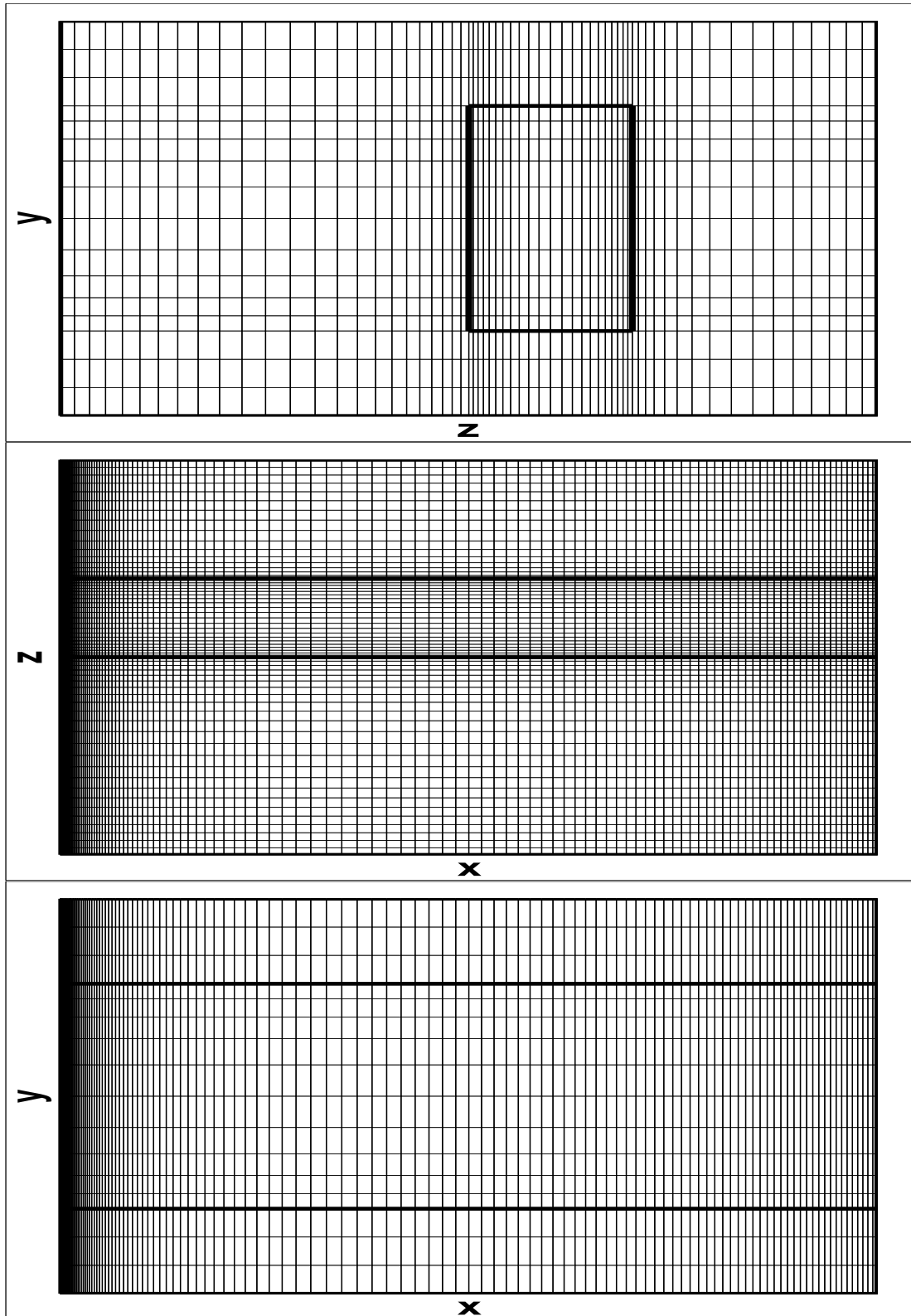


Figure 4.3 x , y and z -Plane Mesh of Microchannel Geometry

For the flow of interest in this problem, continuum flow assumption is valid and Navier-Stokes equations can be used as in reference [42]. The only different

approach used in simulations between the current work and reference [42] is that the properties such as viscosity and thermal conductivity were assumed to be constant in this work, whereas Fedorov and Viskanta modeled the change of fluid properties with temperature.

For the flow solution, no slip boundary condition was applied on the walls. At the inlet, uniform flow velocity in x -direction depending on Reynolds number was given. Velocity components in other two directions were set to zero. In Reynolds number calculation; properties of fluid (water) were taken at 20° C, which is the inlet temperature as stated in [46]. For the exit of the channel, assuming the flow is hydrodynamically fully developed, pressure and tangential velocity components were given as zero. Properties of fluid used in flow computations and hydraulic diameter are given in Table 4.2.

Table 4.2 Properties of Fluid Used in Flow Calculations

D_h	ρ_{water}	μ_{water}
86.6 μm	998.2 kg/m^3	$10^{-3} Pa.s$

In the first flow solutions obtained with the developed code, backflow occurred at the exit of the channel and therefore, a problem with conservation of mass was observed. This was expected since it was stated by Heys et al. that LSFEM encounters continuity problems in high aspect ratio channels such as the current microchannel geometry [19]. Therefore, as described in Chapter 1, it was decided to use weighting of the continuity equation as proposed by Deang and Gunzburger [18] and coefficients of continuity were multiplied with 10 initially. The results obtained with this initial trial were satisfactory and no loss of mass was experienced.

In Figure 4.4 calculated Poiseuille's constant is compared with the data available from experimental work of Kawano et al., analytical result taken from again Kawano et al.'s work and two numerical studies. In addition, to provide further comparison, simulation with commercial code Fluent was conducted using the same mesh created for the developed code. As can be seen from Figure 4.4, there is a high consistency between the data obtained by the current code and Fluent. Furthermore, all the obtained results with LSFEM lie within the experimental uncertainty. Although the

increase of Poiseuille's constant with Reynolds number was found a bit less than experimental findings and what reference [42] predicted, the difference is not too large. Li et al. [67] overestimated the Poiseuille's constant for low Reynolds number and could not model the increase of it with Reynolds number.

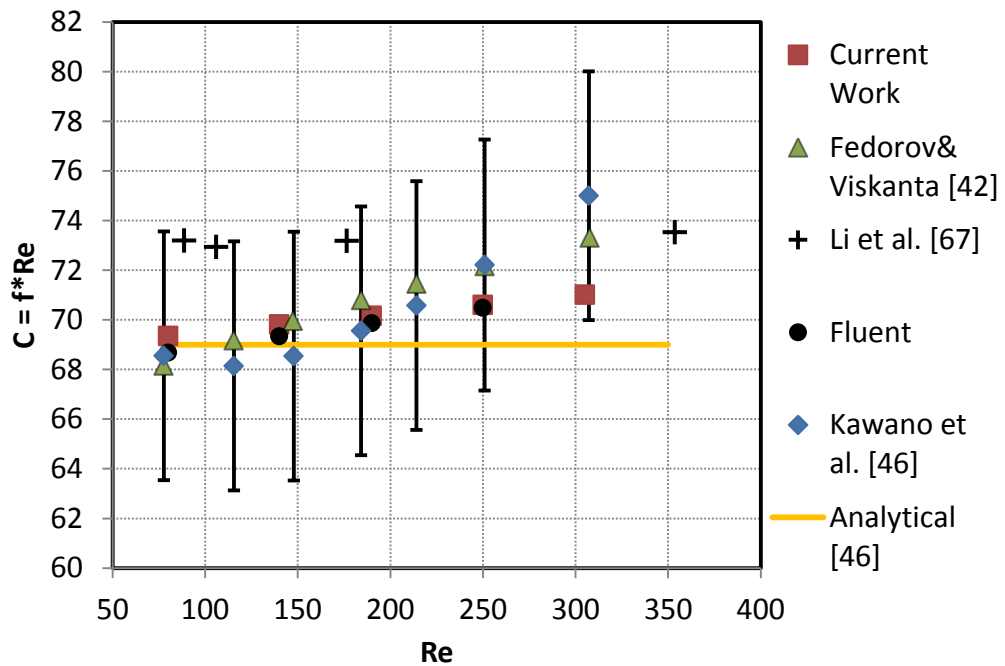


Figure 4.4 Change of Poiseuille's Constant with Reynolds Number

It should be noted that, according to the theory, the Poiseuille's constant should not change with Reynolds number for the fully developed region as can be seen from the analytical result in Figure 4.4. However, both the experimental and numerical results show a dependency on Re, which can be explained by the existence of the flow development region at the entrance of channel. For all the Reynolds numbers simulated, the length of flow development region is less than 1 mm.

In order to examine the effect of weighting of the continuity equation, weights of 3 and 100 were also tried, in addition to the initial value of 10. It was observed that simulation with different weights all converged to the same pressure drop values. However, as the weight increased the convergence rate increased, too.

After solving the flow field, obtained velocity values were used for the heat transfer simulations. As stated earlier, water enters into the channel with a temperature of 20°C. All the external walls except the right z wall were assumed to be perfectly insulated. Therefore, heat fluxes normal to the surfaces were set to zero as thermal boundary condition. A heat flux of 90 W/cm² coming into the domain was applied from the right z wall. At the exit of the flow, either nothing as specified or temperature gradient and hence the heat flux in x -direction was taken as zero. Both boundary conditions for the fluid exit converged to the same temperature distributions. Since the temperature of the domain increases through the end of the domain, fluid and solid (water and silicon) properties were calculated at an estimated average temperature of 300 K. Water and silicon properties used in conjugate heat transfer calculations are given in Table 4.3.

Table 4.3 Properties of Materials Used in Heat Transfer Calculations

$c_{p_{water}}$	k_{water}	ρ_{water}	$k_{silicon}$
4181 J/kg.K	0.61 W/m.K	997 kg/m ³	149 W/m.K

As stated earlier in several times, the heat transfer in fluid and solid regions was solved together and no special treatment was applied at the fluid-solid interfaces. Since the velocities at the solid parts were zero, convection-conduction equation reduced to pure conduction equation for the solid parts automatically. Only the thermal conductivities should be changed in the differential operators depending on the material.

Thermal resistances from the experimental and other numerical works were compared with the ones obtained with the current study. Thermal resistance is defined as

$$R_t = (T_s - T_i)/q_w \quad 4.2$$

where $T_i = 20$ °C is the constant inlet temperature, $q_w = 90$ W/cm² is the specified heat flux at the right z wall and T_s is the surface temperature at the coordinates $x = L$ and $z = W_z^r$. Figure 4.5 shows the thermal resistance comparison.

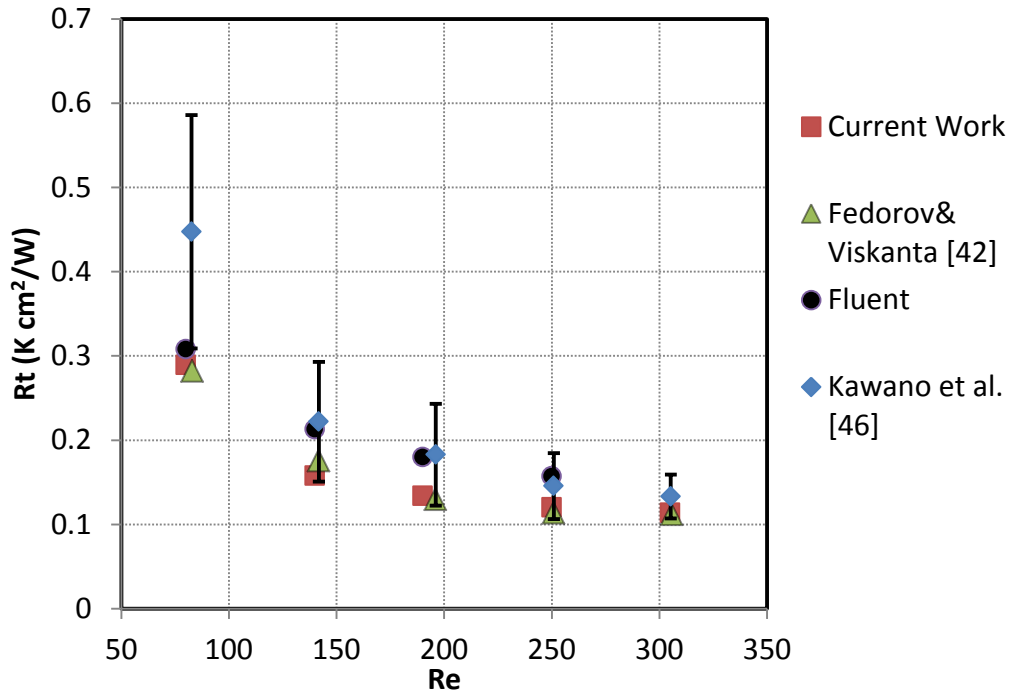


Figure 4.5 Change of Thermal Resistance with Reynolds Number

As can be seen from Figure 4.5, the closest results to the experiments were obtained with the commercial code Fluent. Although the present work underpredicted the thermal resistance values compared to experiments, the results are in experimental uncertainty except for $Re = 80$ and very close to, even better than, the results of Fedorov and Viskanta [42]. Kawano et al. [46] indicated that for $Re = 80$, the flow velocities are too low that all the experimental uncertainties cannot be estimated. This explains why all numerical solutions including the current one failed to predict the thermal resistance for Reynolds number of 80. In addition, the change of thermal resistance with Reynolds number was modeled successfully in the present work.

In addition to thermal resistance, Fedorov and Viskanta [42] also gave bulk temperature, interface temperature and interface heat flux values. These temperature and heat flux results of the current study and Fluent were again compared with that of Fedorov and Viskanta. The change of bulk temperature in x direction is given in Figure 4.6

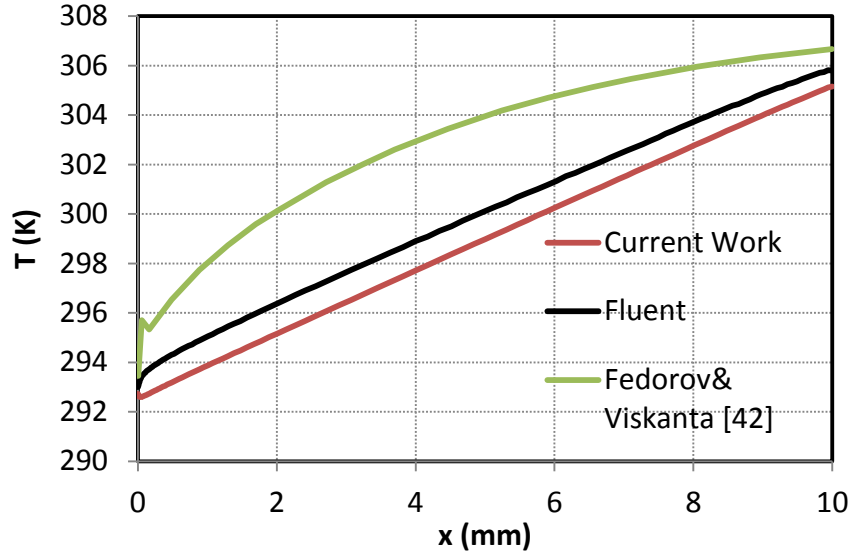


Figure 4.6 Change of Bulk Temperature in x -Direction

The bulk temperature was calculated using Eqn. (4.3).

$$T_b(x) = \frac{\int_{-H_y/2}^{H_y/2} \int_{-H_z/2}^{H_z/2} u T(x, y, z) dz dy}{\int_{-H_y/2}^{H_y/2} \int_{-H_z/2}^{H_z/2} u dz dy} \quad 4.3$$

Similarly, average interface temperatures on y and z walls were calculated using Eqn. (4.4) and Eqn. (4.5).

$$T_y(x) = \frac{\int_{-H_z/2}^{H_z/2} T(x, y = H_y/2, z) dz}{H_z} \quad 4.4$$

$$T_z(x) = \frac{\int_{-H_y/2}^{H_y/2} T(x, y, z = H_z/2) dz}{H_y} \quad 4.5$$

Interface temperature comparisons are given in Figure 4.7.

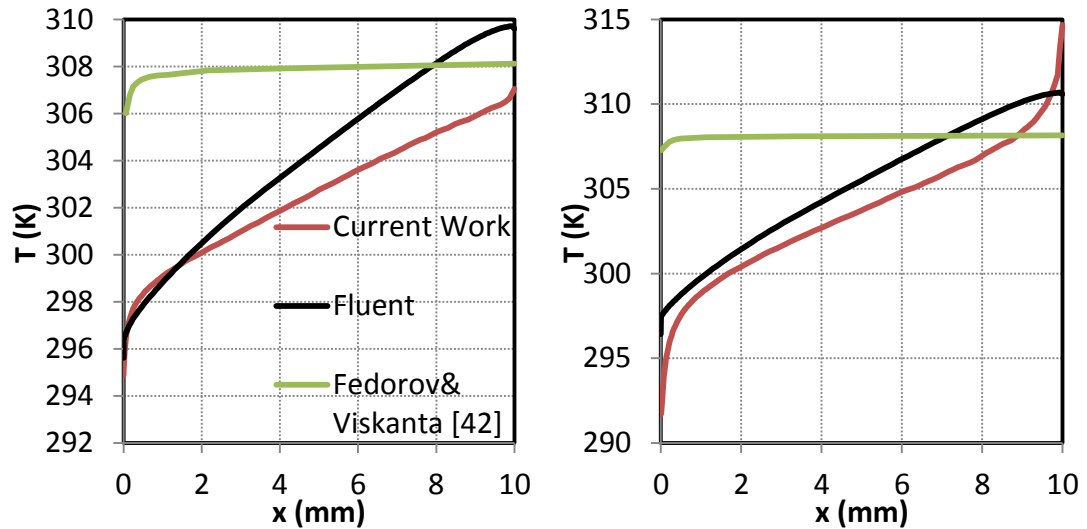


Figure 4.7 Change of Interface Temperatures in x -Direction ($y = H_y/2$ Wall on Left and $z = H_z/2$ Wall on Right)

Considering the bulk temperature comparisons, the results from the current study and Fluent have similar trends whereas results of Fedorov and Viskanta [42] have a different one. Bulk temperature increases with x linearly in the current study and Fluent. However, Fedorov and Viskanta predicted the change of bulk temperature with x as a curve. Their bulk temperature result is likely to converge some temperature value if the length of the channel is long enough. Since there is a constant heat flux applied to the system, this curved behavior of the bulk temperature of Fedorov and Viskanta's work seem to be wrong. There is a slight difference in the results of Fluent and current work and this difference keeps constant through the end of domain.

Although the trends of the current work and that of Fedorov and Viskanta are a little different for bulk temperature, the difference for interface temperature trends is enormous. The interface temperature increases sharply at the inlet portion of the channel and then remains constant till the end in the solution of Fedorov and Viskanta. However, interface temperatures increase almost linearly in the current and Fluent results. The increase of interface temperature on $y = H_y/2$ wall is less in the current study than Fluent's calculation. Although the temperature profiles on $z = H_z/2$ wall are similar for Fluent and the current results in general, there occurred large jumps at the inlet and exit of the domain in the current study. To judge

whether the linear increase of interface temperature as in Fluent and current results or the constant interface temperature as in Fedorov and Viskanta's work is the correct behavior, it is better to observe the heat flux results at the interfaces, too. Natural logarithms of heat fluxes on the interfaces are given in Figure 4.8.

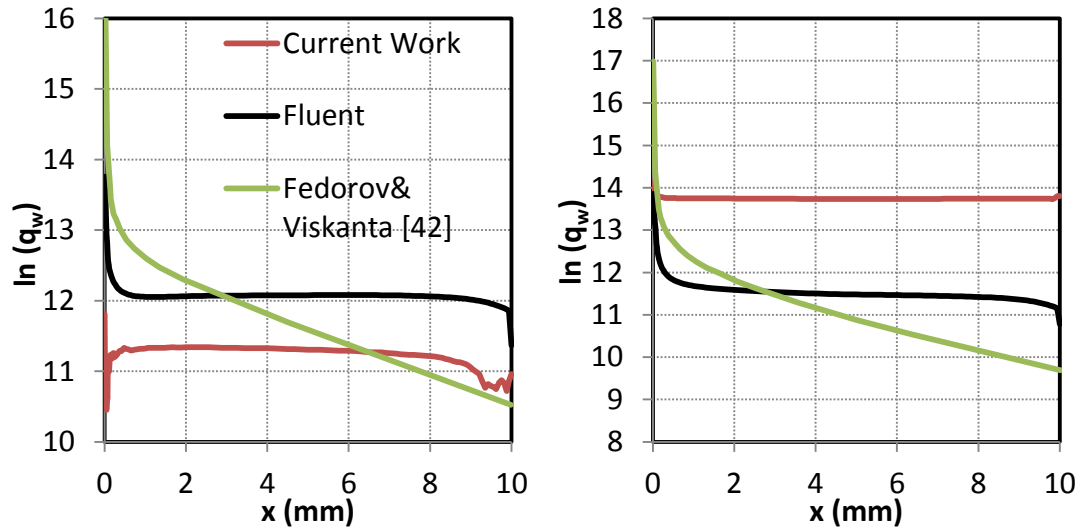


Figure 4.8 Change of Interface Heat Fluxes into the Fluid in x -Direction ($y = H_y/2$ Wall on Left and $z = H_z/2$ Wall on Right)

The large difference in trends between the current solution and that of Fedorov and Viskanta is present in the interface heat fluxes, too. In the current results and Fluent results, heat flux into the fluid domain through interface is almost constant in most of the domain. However, the heat flux drops linearly in the solution of Fedorov and Viskanta. Considering the bulk and interface temperatures together with heat fluxes in Fedorov and Viskanta's work, it is like the bulk temperature will eventually reach the interface temperature and the interface heat flux will drop to zero. This seems to be nonsense since there is a constant heat flux flowing into the domain on the outer wall. In some other works in the literature such as that of Toh et al. [47] and Li et al. [67], the temperature values at the fluid-solid interface increase in axial direction as well. Therefore, temperature and heat flux calculations of Fedorov and Viskanta may be inaccurate and checking the correctness of the current work by comparing the results with that of Fedorov and Viskanta may lead to improper conclusions.

Comparing the results of interface heat flux of Fluent and the current code, it is seen that the heat flux in z direction exceeded the heat flux in y direction in the current results whereas they were almost equal in Fluent's calculations. This difference stems from different calculations of conduction in the Silicon with the current code and Fluent. In the current solution, heat flux coming from the outer z wall went all way to the fluid without changing its direction much whereas in Fluent, the heat flux went through side ways in the solid first and then penetrates into the fluid from all interfaces. Considering relatively high thermal conductivity of Silicon, the Fluent's solution seems more probable. On the other hand, looking at sharp increases or decreases and wiggly results in interface temperatures and heat fluxes, it is certain that the inlet and exit portions of the domain were problematic in the current simulations.

It should be noted that although the flow velocities were not large, the numerical values of convective terms in energy equation were very high due to high density and specific heat values of water. Therefore, it was difficult to obtain satisfactory convergence rates since the fluid and solid parts were solved in a fully coupled fashion. One should think about two adjacent solid and fluid elements to understand the numerical difficulty. At one cell, there is a high diffusion due to high thermal conductivity of Silicon whereas at the adjacent cell, diffusion rates decrease considerably and convection pops up in enormous amounts. Since all the system was solved at once, this sudden increase and decreases resulted in high condition numbers for resulting coefficient matrices.

In conclusion for the microchannel heat transfer simulations, although the Poiseuille's constant and the thermal resistances are predicted successfully, temperature and heat flux values at the interfaces reveal that further simulations should be conducted for some other microchannel configurations in the literature and the accuracy of the current solvers should be examined broadly.

It is also worth mentioning that the microchannel configuration is capable of removing heat at the rates of 90 W/cm^2 even at small Reynolds numbers, with really small thermal resistances. In addition, dimensions of the microchannel geometry are

extremely small that even the tiny microchips can be cooled properly. These prove that the microchannels are efficient and reliable devices to be used in microchip cooling.

CHAPTER 5

CONCLUSIONS AND DISCUSSIONS

In this thesis research, development of a conjugate heat transfer solver based on least squares finite element method was aimed. Since the investigation of heat transfer characteristics of microchannels is one of the progressing engineering areas in which conjugate heat transfer phenomenon occurs, the ultimate goal was selected as modeling microchannel heat transfer with the developed solver. To achieve this goal, firstly the necessary formulation and methodologies to develop solvers were determined. Then, developed solvers were validated by simulating some previously solved problems and by comparing the current results with the ones found in the literature. Finally, a real life microchannel configuration which had been previously examined both experimentally and numerically was found and simulated. The findings compared well in general with the data from other works.

Since the changes of velocity magnitudes in the problems simulated in this study were low, viscous dissipation could be neglected and energy equations could be simplified to convection-conduction equation. Further assuming that the fluid properties such as viscosity and density are independent of temperature, fluid flow and heat transfer parts could be solved separately. Therefore, the fluid flow was solved first and then velocity values were exported to the heat transfer solver to be used in convective part of the energy equation. On the other hand, fluid flow and heat transfer equations were coupled in simulating natural convection since the change of density with temperature was modeled for gravitational forces following the approximation of Boussinesq.

In the flow solver part, velocity-vorticity-pressure first order system was used. Jiang's [5] advice about inclusion of divergence of vorticity equation as an extra equation in order to satisfy the ellipticity of Navier-Stokes equation system was not followed. Trials with and without the divergence of vorticity equation showed that both versions gave the same results, but the convergence rates for the excluded version were higher.

In LSFEM formulation of the energy part, heat flux was defined in order to reduce the system of differential equations to first order. The critical part in forming heat transfer equations was whether the curl of heat flux equation should be added to the system or not. Jiang [16] claimed that curl of heat flux should be included in the system and, Dennis and Dulikravich [13] supported this claim in their work. Again, the trials with the current code showed that inclusion of curl of heat flux equation increases convergence speeds and hence, the included version was used in heat transfer solutions. However, in the natural convection solver where fluid flow and heat transfer were coupled, the work of Tang and Tsang [12] was followed and curl of heat flux and divergence of vorticity equations were not included.

For conjugate heat transfer part of the solver, a fully coupled approach was used as advised by Reddy for FEM based solvers [41]. In this approach, elemental systems from both fluid and solid regions were assembled into the same global system and solved simultaneously. This way, continuity of both the heat flux and temperature at the fluid-solid interface was satisfied automatically and no additional care was taken.

LSFEM is known to have local mass conservation problems. In high aspect ratio channels, even the global mass conservation may not be achieved in flow solutions with LSFEM [19]. This problem was encountered during the simulation of microchannel flow. In order to solve the problem, simple weighting of the continuity equation was performed as advised by Deang and Gunzburger [18]. The results obtained with this approach were satisfactory and used in flow simulations where problems with mass conservation were faced.

Although the fully coupled approach adopted in conjugate heat transfer simulations provide easy treatment, there might occur problems if the convective parts of the energy equation become dominant numerically. Indeed, microchannel heat transfer simulations suffered from this situation. Due to water's high thermal capacity and density, the convection part of the energy equation had high values although the flow velocities were relatively low. On the other hand, solid region was highly conductive due to the relatively high thermal conductivity of Silicon. When the elemental systems written for each medium were assembled into one global system, condition number of the resultant coefficient matrix became high. Therefore, it took too many iterations to obtain converged solutions.

The current study may be improved in many ways. These are left as possible future works and may be listed as:

- Making the solver applicable to unsteady problems. This way, both the real transient problems may be solved and a time marching approach may be used for steady state problems.
- Adopting the incomplete Cholesky factorization as the preconditioner of the conjugate gradient solver and comparing the new version with the current Jacobi preconditioner in terms of CPU times.
- Handling the conjugate heat transfer problems in a separated fashion for fluid and solid media and comparing the results of the new method with the current fully coupled version.
- Overcoming the problems related to the usage of tetrahedron elements and hence, being able to create meshes more flexibly.
- Simulating more microchannel heat transfer problems to further validate the solver. This way, the solver can be used confidently as a computational tool for real engineering applications where conjugate heat transfer occurs.

Although there are certain problems that may arise in the application of LSFEM, these problems may be overcome easily with special care and necessary precautions. Considering the advantages like resulting sparse, symmetric and positive definite matrices and applicability to all kinds of flow regimes; LSFEM still stands as a promising research area which deserves further investigation. As for the developed

solver; it can serve as a useful tool in simulation of conjugate heat transfer phenomenon in a wide variety of engineering applications with the future improvements and added features.

REFERENCES

- [1] Least-Squares Finite Element Methods, <http://people.sc.fsu.edu/~mgunzburger/fem/ls.html> last visited on August 2012.
- [2] Kayser-Herold, O., and Matthies, H. G., 2005, "Least-Squares FEM Literature Review", Report No. 2005-05, Technical University Braunschweig, Brunswick, Germany
- [3] Zienkiewicz, O.C., 1996, "Origins, Milestones and Directions of the Finite Element Method-A Personal View", *Handbook of Numerical Analysis*, **4**, pp. 3-67.
- [4] Bochev, P.B., and Gunzburger, M.D., 2009, *Least-squares finite element methods*, Springer, NY, USA.
- [5] Jiang, B., 1998, *The Least-Squares Finite Element Method: Theory and Applications in Computational Fluid Dynamics and Electromagnetics*, Springer, NY, USA.
- [6] Jiang, B., 1992, "A Least-Squares Finite Element Method for Incompressible Navier-Stokes Problems," *International Journal for Numerical Methods in Fluids*, **14**(7) pp. 843-859.
- [7] Tang, L. Q., Cheng, T., and Tsang, T. T. H., 1995, "Transient Solutions for three-dimensional lid-driven Cavity Flows by a least-squares Finite Element Method," *International Journal for Numerical Methods in Fluids*, **21**(5) pp. 413-432.
- [8] Pontaza, J. P., 2006, "A Least-Squares Finite Element Formulation for Unsteady Incompressible Flows with Improved velocity–pressure Coupling," *Journal of Computational Physics*, **217**(2) pp. 563-588.
- [9] Bochev, P. B., and Gunzburger, M. D., 1995, "Least-Squares Methods for the Velocity-Pressure-Stress Formulation of the Stokes Equations," *Computer Methods in Applied Mechanics and Engineering*, **126**(3–4) pp. 267-287.
- [10] Chang, C. L., 1990, "A Mixed Finite Element Method for the Stokes Problem: An Acceleration-Pressure Formulation," *Applied Mathematics and Computation*, **36**(2) pp. 135-146.
- [11] Bochev, P., 1997, "Experiences with Negative Norm Least–Square Methods for the Navier–Stokes Equations," *Electronic Transactions on Numerical Analysis*, **6**pp. 44-62.

- [12] Tang, L. Q., and Tsang, T. T. H., 1993, "A Least-Squares Finite Element Method for Time-Dependent Incompressible Flows with Thermal Convection," *International Journal for Numerical Methods in Fluids*, **17**(4) pp. 271-289.
- [13] Dennis, B., and Dulikravich, G., 2000, "Simulation of Magnetohydrodynamics with Conjugate Heat Transfer," *Proceedings of ECCOMAS2000-European Congress on Computational Methods in Applied Sciences and Engineering*, Barcelona, pp. 11-14.
- [14] Romao, E.C., Aparecido, J. B., Campos-Silva, J. B., de Moura, L. F. M., 2009, "GFEM and LSFEM in the Solution of the Transient Bidimensional Convection-Diffusion Equation," *Engenharia Termica*, **8**(01) pp. 36-43.
- [15] BOCHEV, P. B., 1994, "Least Squares Finite Element Methods for the Stokes and Navier-Stokes Equations," PhD thesis, Virginia Polytechnic Institute and State University.
- [16] Jiang, B. N., and Povinelli, L. A., 1993, "Optimal Least-Squares Finite Element Method for Elliptic Problems," *Computer Methods in Applied Mechanics and Engineering*, **102**(2) pp. 199-212.
- [17] Heys, J. J., Lee, E., Manteuffel, T. A., 2007, "An Alternative Least-Squares Formulation of the Navier–Stokes Equations with Improved Mass Conservation," *Journal of Computational Physics*, **226**(1) pp. 994-1006.
- [18] Deang, J., and Gunzburger, M., 1998, "Issues Related to Least-Squares Finite Element Methods for the Stokes Equations," *SIAM Journal on Scientific Computing*, **20**(3) pp. 878-906.
- [19] Heys, J., Lee, E., Manteuffel, T., 2006, "On Mass-Conserving Least-Squares Methods," *SIAM Journal on Scientific Computing*, **28**(5) pp. 1675-1693.
- [20] Heys, J., Lee, E., Manteuffel, T., 2009, "Enhanced Mass Conservation in Least-Squares Methods for Navier–Stokes Equations," *SIAM Journal on Scientific Computing*, **31**(3) pp. 2303-2321.
- [21] Jiang, B., and Chang, C. L., 1990, "Least-Squares Finite Elements for the Stokes Problem," *Computer Methods in Applied Mechanics and Engineering*, **78**(3) pp. 297-311.
- [22] Bochev, P. B., and Gunzburger, M. D., 1994, "Analysis of Least Squares Finite Element Methods for the Stokes Equations," *Mathematics of Computation*, **63**(208) pp. 479-506.
- [23] Chang, C. L., and Yang, S., 2002, "Analysis of the L2 Least-Squares Finite Element Method for the velocity–vorticity–pressure Stokes Equations with Velocity Boundary Conditions," *Applied Mathematics and Computation*, **130**(1) pp. 121-144.

- [24] Jiang, B., and Povinelli, L. A., 1990, "Least-Squares Finite Element Method for Fluid Dynamics," *Computer Methods in Applied Mechanics and Engineering*, **81**(1) pp. 13-37.
- [25] Winterscheidt, D., and Surana, K. S., 1994, "P-version Least Squares Finite Element Formulation for two-dimensional, Incompressible Fluid Flow," *International Journal for Numerical Methods in Fluids*, **18**(1) pp. 43-69.
- [26] Bolton, P., and Thatcher, R. W., 2006, "A Least-Squares Finite Element Method for the Navier–Stokes Equations," *Journal of Computational Physics*, **213**(1) pp. 174-183.
- [27] Pontaza, J. P., and Reddy, J. N., 2006, "Least-Squares Finite Element Formulations for Viscous Incompressible and Compressible Fluid Flows," *Computer Methods in Applied Mechanics and Engineering*, **195**(19–22) pp. 2454-2494.
- [28] Taghaddosi, F., Habashi, W. G., Guèvremont, G., 1999, "An Adaptive Least-Squares Method for the Compressible Euler Equations," *International Journal for Numerical Methods in Fluids*, **31**(7) pp. 1121-1139.
- [29] Guaily, A. G. M., 2006, "Directionally Adaptive Least Squares Finite Element Method for the Compressible Euler Equations", Cairo University, Cairo, Egypt.
- [30] Akargün, H. Y., 2012, "Least-squares Finite Element Solution of Euler Equations with Adaptive Mesh Refinement", M.S. Thesis, Middle East Technical University, Ankara, Turkey.
- [31] Donea, J., and Quartapelle, L., 1992, "An Introduction to Finite Element Methods for Transient Advection Problems," *Computer Methods in Applied Mechanics and Engineering*, **95**(2) pp. 169-203.
- [32] Ding, X., and Tsang, T. T. H., 2001, "Large Eddy Simulation of Turbulent Flows by a Least-Squares Finite Element Method," *International Journal for Numerical Methods in Fluids*, **37**(3) pp. 297-319.
- [33] Edgar, N. B., and Surana, K. S., 1994, "P-Version Least Squares Finite Element Formulation for Axisymmetric Incompressible Non-Newtonian Fluid Flow," *Computer Methods in Applied Mechanics and Engineering*, **113**(3–4) pp. 271-300.
- [34] Kayser-Herold, O., and Matthies, H. G., 2005, "Least Squares Finite Element Methods for Fluid-Structure Interaction Problems," *Computers & Structures*, **83**(2–3) pp. 191-207.
- [35] Heys, J. J., Manteuffel, T. A., McCormick, S. F., 2004, "First-Order System Least Squares (FOSLS) for Coupled Fluid-Elastic Problems," *Journal of Computational Physics*, **195**(2) pp. 560-575.

- [36] Wansophark, N., Malatip, A., and Dechaumphai, P., 2005, "Streamline Upwind Finite Element Method for Conjugate Heat Transfer Problems," *Acta Mechanica Sinica*, **21**(5) pp. 436-443.
- [37] Patankar, S.V., 1980, *Numerical heat transfer and fluid flow*, Hemisphere Pub, USA.
- [38] Hriberšek, M., and Kuhn, G., 2000, "Conjugate Heat Transfer by Boundary-Domain Integral Method," *Engineering Analysis with Boundary Elements*, **24**(4) pp. 297-305.
- [39] Divo, E., Steinthorsson, E., Kassab, A. J., and Bialecki, R., 2002, "An iterative BEM/FVM protocol for steady-state multi-dimensional conjugate heat transfer in compressible flows," *Engineering Analysis with Boundary Elements*, **26**(5), pp. 447–454.
- [40] White, F.M., 1991, *Viscous Fluid Flow*, McGraw-Hill, New York, NY .
- [41] Reddy, J.N., and Gartling, D.K., 2010, *The Finite Element Method in Heat Transfer and Fluid Dynamics*, CRC, Florida.
- [42] Fedorov, A. G., and Viskanta, R., 2000, "Three-Dimensional Conjugate Heat Transfer in the Microchannel Heat Sink for Electronic Packaging," *International Journal of Heat and Mass Transfer*, **43**(3) pp. 399-415.
- [43] Ateş, A. M., 2011, "Experimental Comparison of Fluid and Thermal Characteristics of Microchannel and Metal Foam Heat Sinks," M.S. Thesis, Middle East Technical University, Ankara, Turkey.
- [44] Alpsan, E., 2008, "Experimental Investigation and Numerical Analysis of Microchannel Heatsinks for Phased Array Radar Cooling Applications," M.S. Thesis, Middle East Technical University, Ankara, Turkey.
- [45] Tuckerman, D. B., 1984, "Heat-Transfer Microstructures for Integrated Circuits," Ph.D. Thesis, University of California, Livermore, California.
- [46] Kawano, K., Sekimura, M., Minakami, K., 2001, "Development of Micro Channel Heat Exchanging," *JSME International Journal Series B*, **44**(4) pp. 592-598.
- [47] Toh, K., Chen, X., and Chai, J., 2002, "Numerical Computation of Fluid Flow and Heat Transfer in Microchannels," *International Journal of Heat and Mass Transfer*, **45**(26) pp. 5133-5141.
- [48] Xie, X., Liu, Z., He, Y., 2009, "Numerical Study of Laminar Heat Transfer and Pressure Drop Characteristics in a Water-Cooled Minichannel Heat Sink," *Applied Thermal Engineering*, **29**(1) pp. 64-74.
- [49] Kays, W.M. and Crawford, M.E., 1993, *Convective Heat and Mass Transfer*, McGraw-Hill, Highstown, NJ.

- [50] Sert, C., 2010, "ME582 Lecture Notes", Middle East Technical University, Ankara, Turkey.
- [51] Zienkiewicz, O. C., Taylor, R. L., Zhu, J. Z., 2005, *The Finite Element Method: Its Basis and Fundamentals*, Elsevier, Oxford, UK.
- [52] Fluent Inc., 2006, "Gambit Tutorial Guide," Lebanon, NH, pp. C21-C34
- [53] Shewchuk, J. R., 1994, "An Introduction to the Conjugate Gradient Method without the Agonizing Pain," Carnegie Mellon University, Pittsburgh, PA.
- [54] Bai, Z., Demmel, J., Dongarra, J., Ruhe, A. and van der Vorst, H., 2000, *Templates for the Solution of Algebraic Eigenvalue Problems: A Practical Guide*. SIAM, Philadelphia.
- [55] Intel Math Kernel Library – Documentation, <http://software.intel.com/en-us/articles/intel-math-kernel-library-documentation> last visited on September 2012.
- [56] Yang, J. Y., Yang, S. C., Chen, Y. N., 1998, "Implicit Weighted ENO Schemes for the Three-Dimensional Incompressible Navier–Stokes Equations," *Journal of Computational Physics*, **146**(1) pp. 464-487.
- [57] Zunic, Z., Hribersek, M., Skerget, L., 2006, "3D Lid Driven Cavity Flow by Mixed Boundary and Finite Element Method," *European Conference on Computational Fluid Dynamics*, TU Delft, The Netherlands.
- [58] Albensoeder, S., and Kuhlmann, H., 2005, "Accurate Three-Dimensional Lid-Driven Cavity Flow," *Journal of Computational Physics*, **206**(2) pp. 536-558.
- [59] Armaly, B., Durst, F., Pereira, J., 1983, "Experimental and Theoretical Investigation of Backward-Facing Step Flow," *Journal of Fluid Mechanics*, **127**(1) pp. 473-496.
- [60] Williams, P., and Baker, A., 1997, "Numerical Simulations of Laminar Flow Over a 3D backward-facing Step," *International Journal for Numerical Methods in Fluids*, **24**(11) pp. 1159-1183.
- [61] Jiang, B. N., Hou, L. J., Lin, T. L., Povinelli, L. A., 1995, "Least-Squares Finite Element Solutions for Three-Dimensional Backward-Facing Step Flow," *International Journal of Computational Fluid Dynamics*, **4**(1-2) pp. 1-19.
- [62] Ku, H. C., Hirsh, R. S., Taylor, T. D., 1989, "A Pseudospectral Matrix Element Method for Solution of Three-Dimensional Incompressible Flows and its Parallel Implementation," *Journal of Computational Physics*, **83**(2) pp. 260-291.
- [63] Wakashima, S., and Saitoh, T. S., 2004, "Benchmark Solutions for Natural Convection in a Cubic Cavity using the High-Order time–space Method," *International Journal of Heat and Mass Transfer*, **47**(4) pp. 853-864.

- [64] Bilski, S., Lloyd, J., and Yang, K., 1986, "An Experimental Investigation of the Laminar Natural Convection Velocity in Square and Partitioned Enclosures," *Proc. 8th Int. Heat Transfer Conf*, **4**, pp. 1513-1518.
- [65] Krane, R., and Jessee, J., 1983, "Some Detailed Field Measurements for a Natural Convection Flow in a Vertical Square Enclosure," *Proceedings of the First ASME–JSME Thermal Engineering Joint Conference*, **1**, pp. 323-329.
- [66] Fusegi, T., Hyun, J. M., and Kuwahara, K., 1991, "A Numerical Study of 3D Natural Convection in a Cube: Effects of the Horizontal Thermal Boundary Conditions," *Fluid Dynamics Research*, **8**(5) pp. 221-230.
- [67] Li, J., Peterson, G., and Cheng, P., 2004, "Three-Dimensional Analysis of Heat Transfer in a Micro-Heat Sink with Single Phase Flow," *International Journal of Heat and Mass Transfer*, **47**(19) pp. 4215-4231.